Modeling volcanic ash aggregation processes and related impacts on the April/May 2010 eruptions of Eyjafjallajökull Volcano with WRF-Chem.

Sean D. Egan[1], Martin Stuefer[2], Peter W. Webley[2], Taryn Lopez[2], Catherine F. Cahill[2], Marcus Hirtl[3]

[1]Department of Chemistry, University of Alaska Fairbanks, Fairbanks, AK, 99775, USA
[2]Geophysical Institute, University of Alaska Fairbanks, Fairbanks, AK 99775, USA
[3]Department of Chemical Weather Forecasting, Zentralanstalt für Meteorologie und Geodynamik (ZAMG), Wien, 1190, AT

Correspondence to: Sean D. Egan (sdegan@alaska.edu, sean.d.egan@navy.mil)

Abstract. Volcanic eruptions eject ash and gases into the atmosphere that can contribute to significant hazards to aviation, public and environment health, and the economy. Several volcanic ash transport and dispersion (VATD) models are in use to simulate volcanic ash transport operationally, but none include a treatment of volcanic ash aggregation processes. Volcanic ash aggregation can greatly reduce the atmospheric budget, dispersion and lifetime of ash particles and therefore its impacts. To enhance our understanding and modeling capabilities of the ash aggregation process, a volcanic ash aggregation scheme was integrated into the Weather Research Forecasting with online Chemistry (WRF-Chem) model. Aggregation rates and ash mass loss in this modified code are calculated in-line with the meteorological conditions, providing a fully coupled treatment of aggregation processes. The updated-model results were compared to field measurements of tephra fallout and in situ airborne measurements of ash particles from the April/May 2010 eruptions of Eyjafjallajökull Volcano, Iceland. WRF-Chem, coupled with the newly added aggregation code, modeled ash clouds that agreed spatially and temporally with these in situ and field measurements. A sensitivity study provided insights into the mechanics of the aggregation code by analyzing each aggregation process (collision kernel) independently, as well as by varying the fractal dimension of the newly formed aggregates. In addition, the airborne lifetime (e-folding) of total domain ash mass was analyzed for a range of fractal dimension, and a maximum reduction of 79.5% of the airborne ash lifetime was noted.

1. Introduction

Volcanic eruptions inject gases and ash particles of various sizes into the atmosphere, posing hazards to life, infrastructure and aviation (Miller and Casadevall, 2000). Volcanic emissions can alter the composition of the atmosphere and affect the Earth's radiation budget and climate (Angell, 1993; Cole-Dai, 2010; Thordarson and Self, 2003). The environmental and economic impacts of past and recent eruptions have spurred increased interest in the inclusion of volcanic ash into numerical weather prediction (NWP) models (Folch et al., 2009, 2015; Lin et al., 2012; Stuefer et al., 2013). Today, forecasters and scientists utilize volcanic ash transport and dispersion (VATD) models for ash hazard mitigation, the

development, calibration and validation of remote sensing tools, and the study of ash physics. Numerical models have been developed to better describe the initial plume characteristics of eruptions, such as the plume height, water content, particle size distribution and plume shape. A current limitation of most VATD models is their ability to capture volcanic ash aggregation.

Volcanic ash aggregation is important for many reasons. Aggregation affects the atmospheric lifetime of ash, the distance ash is transported from the eruption source, the size and type of tephra observed on the ground, and the duration ash poses a threat to aircraft (Brown et al., 2012; Casadevall, 1994; Rose and Durant, 2011). Aggregation has been observed in several well studied volcanic eruptions such as those of Mount St. Helens (Washington), Mount Redoubt (Alaska) and Eyjafjallajökull (Iceland). Additionally, aggregation occurs in both proximal (< 15 km from the plume edge) and distal ash clouds (Bonadonna et al., 2011; Bonadonna and Phillips, 2013; Brown et al., 2012; Carey and Sigurdsson, 1982; Rose and Durant, 2009, 2011; Taddeucci et al., 2011; Wallace et al., 2013).

Proximal volcanic ash aggregates form more rapidly than distal aggregates for a number of reasons. For example, ice and liquid water enhance the sticking of particles and thus increases the rate of aggregation (Brown et al., 2012; Rose and Durant, 2011). This process can occur in a hail-like process with a cycle of freezing and thawing leading to enhanced aggregation (Van Eaton et al., 2015). In addition, the higher concentration of ash in the proximal plume increases the number of collisions.

Water enhanced aggregation in the proximal plume has been observed in a number of eruptions. Field observations of tephra from the May 18, 1980 eruption of Mount St. Helens detail the formation of large volcanic aggregates (up to 1mm) closely correlated with the presence of rain, snow, and hail (Waitt et al., 1981). Gilbert and Lane (1994) note that aggregation rates were enhanced by high proximal water vapor concentrations during the eruptions of Sakurajima volcano in the 1990s, and the majority of this water-enhanced aggregation occurred proximally, within the first minutes of the eruption. In addition, studies of the 2009 eruption of Mount Redoubt in Alaska show definitive evidence for aggregation enhanced sedimentation in the proximal plume (Van Eaton et al., 2015; Wallace et al., 2013). Van Eaton et al. (2015) conclude that the effects of aggregation in the Redoubt eruption resulted in over 95% of fine ash mass deposited to the ground as aggregates.

Distal aggregation usually occurs at a slower rate than proximal aggregation as the plume ages and diffuses (Rose and Durant, 2009, 2011). Despite a slower rate of aggregation the majority of distal fine ash settles to the ground as larger aggregates (Brown et al., 2012; Carey and Sigurdsson, 1982; Rose and Durant, 2011; Wallace et al., 2013). Both coarse and fine ash particles are known to aggregate in distal clouds by forming dry clusters due to electrostatic attraction, or as liquid or frozen water particles (Brown et al., 2012; Rose and Durant, 2011). Distal aggregate formation has been observed from eruptions such as Etna Volcano, Italy in 1971, Mount St. Helens, U.S. in 1980 and Mount Redoubt, U.S. in 1990 (Booth and Walker, 1973; Sorem, 1982; Sparks et al., 1997). For many eruptions, electrostatic aggregation of fine ash is expected to be responsible for the bimodal distribution of volcanic ash fallout (Carey and Sigurdsson, 1982; Cornell et al., 1983; James et al., 2003).

Commented [SDE1]: Adding these parameters as requested by Reviewer 2

Deleted: corner

Recently, aggregation processes were observed to play an integral role in the dispersion of the plume generated from the April and May 2010 eruptions of Eyjafjallajökull Volcano, Iceland. In-situ measurements of ash particle fall velocities using high speed photography observed aggregation-enhanced sedimentation that increased fallout rates by a factor of 10 (Taddeucci et al., 2011). The effect of ash aggregation caused a significant quantity of additional ash fall across Iceland, rather than be transported further. Ash aggregation overall clearly reduced the atmospheric residency time of the Eyjafjallajökull ash plume (Gudmundsson et al., 2012). In addition, aggregation was observed to cause enhanced fallout over parts of mainland Europe and the United Kingdom (Stevenson et al., 2012).

Aggregation processes not only affect the lifetime of volcanic ash, but also the makeup of volcanic ash cloud particle size distributions (PSDs) which may complicate modeling and remote sensing efforts (Brown et al., 2012; Rose and Durant, 2011). For example, volcanic ash remote sensing algorithms require information regarding particle sizes and extinction coefficients (Stohl et al., 2011; Wallace et al., 2013). Remote sensing methods are also used to estimate eruption parameters and PSDs via extinction coefficients using inverse modeling (Kristiansen et al., 2012; Stohl et al., 2011). Additionally, volcanic PSDs are also important for the study of radiative properties of volcanic ash and their effects on the atmosphere (Hirtl et al., 2019; Young et al., 2012).

The effects imposed on volcanic ash clouds by aggregation processes necessitates their parameterization in volcanic ash transport and dispersion (VATD) models. Despite this, only few of the existing VATD models capture aggregation processes. For example, a volcanic ash aggregation parameterization scheme has been implemented within the FALL3D model (Folch et al., 2009). In an operational setting, FALL3D runs by ingesting offline meteorological fields from gridded atmospheric models, such as the Weather Research Forecasting (WRF) model, and then calculating volcanic ash advection and sedimentation during the parent model output time step. Another method of capturing volcanic ash aggregation is to initialize VATD models with PSDs that account for volcanic aggregation in the eruptive column by using initial plume models. FPLUME, a one dimensional (1D) plume model based on buoyant plume theory, constructs initial plume characteristics that account for ash aggregation (Folch et al., 2016). In this case, the 1D plume model develops an initial PSD at the source that accounts for aggregation processes and then keeps this PSD invariant during further plume transport.

In effort to study and predict volcanic ash aggregation effects using a fully coupled modeling system, where the fate of the airborne ash particles is coupled to the atmospheric environment, a volcanic ash aggregation scheme was incorporated into the Weather Research Forecasting with Chemistry (WRF-Chem) model (Grell et al., 2005). This coupled system requires no temporal nor spatial interpolations as it calculates interactions between the meteorology and ash at each modeling time step (on the order of seconds). While many dispersion models require less computing power than WRF, a number of them require a mesoscale model, like WRF, to generate regional, gridded meteorological fields for their initialization. As an example, FALL3D is typically initialized with a WRF model run that is executed prior to the dispersion model. Modeling particle dispersion with WRF-Chem is, therefore, as computationally feasible as running these models since in many cases, a mesoscale, gridded model must be run for their initialization. In addition, volcanic ash aircraft hazard mitigation typically focuses on limiting commercial aircraft to ash concentration thresholds (Casadevall, 1994). WRF-Chem

solves the advection equations such that ash concentration is tracked over time. This ability to track volcanic ash mass, rather than particle number as is done in many VATD particle dispersion models, augments current VATD model guidance and offers another tool to constrain atmospheric ash loading.

The following sections of this paper detail the inclusion of a computationally feasible volcanic ash aggregation scheme into the WRF-Chem model and the impacts of these modifications on model output. The following 'Aggregation Parameterization and Implementation' section (Section 2) details the background and incorporation of a mathematical scheme that is physically descriptive of aggregation processes into WRF-Chem, as well as the development of a new methodology for selecting aggregation sticking efficiencies that depend on relative humidity. This newly implemented code is then applied to the April and May 2010 eruptions of Eyjafjallajokull, as well as to a controlled sensitivity study using a single eruption. The setup of these two cases is discussed in Section 3 'Methods', with remarks on the model output in Section 4 'Results'. Concluding remarks and then provided in the final Section 5 'Conclusions'.

2. Aggregation Parameterization and Implementation

Smoluchowski (1917) developed the original analytical theory of the process of coagulation of colloid particles based upon Prof. R. Zsigmondy's experiments with gold solutions. The Smoluchowski Coagulation Equation (Eq. 1) is an integrodifferential, population balance equation that describes the evolution of particle number density, $n_v(v)$, in time t, as primary particles of one volume, v , collide and stick together with particles of different volumes, v', to form aggregates (Smoluchowski, 1917). It is physically descriptive of the aggregation process.

$$\frac{\partial n_v(v)}{\partial t} = \frac{1}{2}\int_0^v K(v-v', v)\, n_v(v-v')\, n_v(v')\, dv' - n_v(v)\int_0^\infty K(v, v')\, n_v(v')\, dv' \quad (1)$$

Equation (1) describes the number of aggregates of volume v formed, n_v, per unit time, t, on the left, and the loss of primary particles between volumes v and v' on the right as particles aggregate based on the collision frequency of the particles. Frequency is weighted by the coagulation kernel, K, which is the product of the collision kernel, A, and a sticking efficiency, α, thus, $K = A\alpha$.

Volcanic ash may undergo various processes that result in collisions, such as Brownian motion, differential sedimentation and fluid shear, and as a result there are many formulations of the coagulation kernel, K (Jacobson, 2005). For example, collisions due to Brownian interactions (A_B) occur randomly during diffusion and are temperature dependent. As temperature increases, the diffusion rate increases thus increasing their chances of interacting with other particles. Particle collisions due to shear (A_S) occur when ash moving in different horizontal directions collide due to changes in laminar flow. This kernel therefore depends on wind speed and direction. Lastly, differential sedimentation (A_{DS}) captures particle interactions due to the different fall velocities of different sized particles. The rate at which particles settle is dependent on their size and therefore the differential sedimentation kernel depends on the difference in size between particles. As larger particles fall, they have a greater chance of encountering smaller, slower moving particles on their descent. In summary, the

collision kernels A_B, A_S and A_{DS} represent the rate at which ash particles collide based on Brownian motion, fluid shear and differential sedimentation, respectively. Each kernel depends directly on the number concentration and size distribution of ash particles, and each depends highly on its own set of parameters.

While physically descriptive of the aggregation process, the Smoluchowski Equation itself, in addition to the equations governing the coagulation kernel, K, is prohibitively computationally expensive to solve explicitly, even with simple boundary conditions. Advances in simplifying the equation for use in computational volcanic ash modeling resulted in large part from work by Dekkers and Friedlander (2002) and Costa et al. (2010) by assuming a time independent aggregate size distribution and fractal geometry of volcanic ash aggregates, respectively. Assuming a fractal aggregate geometry greatly simplifies the equations describing the coagulation kernels (A_B, A_S and A_{DS}) by establishing a particle size-volume fractal relationship, described by a fractal dimension factor , ξ. In addition, an assumption of fractal geometry allows n_v in Eq. (1) to be described in terms of the total number of particles in a computational space, n_{tot}, forming aggregates of a certain fractal dimension, D_f, based on a generally accepted fractal relationship (Jullien and Botet, 1987; Lee and Kramer, 2004). The simplified Smoluchowski equation described by Costa et al. (2010) results in a calculation of $\frac{\partial n_v(v)}{\partial t}$, from Eq. (1), that is much more computationally feasible (Eq. 2)

$$\Delta n_{tot} = \alpha \left(A_B n_{tot}^2 + A_s \Phi^{\frac{3}{D_f}} n_{tot}^{2-\frac{3}{D_f}} + A_{DS} \Phi^{\frac{4}{D_f}} n_{tot}^{2-\frac{4}{D_f}} \right) \Delta t \quad (2)$$

Here, Δn_{tot} represents the total number of particles per unit volume lost to aggregation. The equation relies on the solid volume fraction of the aggregates, Φ (Folch et al., 2016), the number densities of the bins, n_{tot}, as well as the fractal dimension of the fine ash particles, D_f (Costa et al., 2010). Equations describing the collision kernel, A, were also simplified using a fractal representation of ash geometry and were reduced to Eq. (3) through Eq. (5), shown in Table 1.

New code capable of calculating Eq. (2) to Eq. (5) was developed in this study and integrated into the Fortran 90 module "module_vash_settling.F" file, located in the "chem" subdirectory of the WRF main directory, which is available to download from the WRF homepage: www2.mmm.ucar.edu/wrf/users/downloads.html. Modified code is available upon request. See the following "Code Availability" section for details.

Most of the source variables necessary to solve Eq. (2) to Eq. (5) are available in WRF-Chem by selecting the appropriate aerosol and chemistry packages. For example, chemistry option (chem_opt) 402 (WRF-Chem User Guide 3.9, 2018) includes chemistry and humidity variables provided by the Regional Deposition Acid Model Version 2 (RADM2) (Stockwell et al., 1990) and the Goddard Chemistry Aerosol Radiation and Transport (GOCART) models (Chin et al., 2000), as well as the inclusion of volcanic sulfur dioxide (SO_2) and ten volcanic ash particle size bins (Stuefer et al., 2013). Three variables required by Eq. (2) to Eq. (5), the sticking efficiency, α, fractal dimension, D_f, and fractal dimension factor, ξ are not, however, included in WRF-Chem and therefore must be calculated or assumed.

Commented [SDE2]: Reviewer 2 requested that we include a reference to Table 1 in the main body of the text, which we do here.

The fractal dimension, D_f, relates the number of primary particles N in an aggregate to the size of the aggregate, R, such that N scales proportionally as $N \propto R^{D_f}$. For example, as D_f approaches 3, primary particles in the aggregate use up more and more space such that $D_f = 3.0$ would indicate a solid, filled aggregate. A lack of experimental data adds a degree of uncertainty when selecting the fractal dimension, however previous analysis studies of aggregates selected after the eruptive events from Mount Saint Helens and Mount Spurr suggested a dimension D_f = 2.99. This favorable fractal dimension resulted from a regression analysis between model output and observed deposits (Folch et al., 2010). The fidelity of confidence in the choice of the fractal dimension is hindered by the fact that it does not necessarily, by its definition, remain constant within a plume.

The fractal dimension factor, $\boldsymbol{\xi}$, used to simplify the coagulation kernel equations relates the fractal dimension, D_f, to the diameters and volumes of the primary particles in the aggregates. This relationship is given in Eq. (6)

$$d_i = \xi v_i^{\frac{1}{D_f}} \quad (6)$$

Deleted: 3

Here, d_i and v_i are the diameter and volume of the primary particles forming an aggregate. Costa et al. (2010), Dekkers and Friedlander, (2002) and Folch et al. (2010) indicate that a fractal dimension on the order of 0.6 to 1 is sufficient for describing the geometry of volcanic ash particles and aggregates. As done in Costa et al. (2010), a unity fractal dimension factor is utilized in this study.

The sticking efficiency coefficient, α, relies heavily on the concentration of water vapor and ice (Costa et al., 2010). In order to formulate an appropriate estimate for the sticking efficiency coefficient, a new parameterization was incorporated into the WRF-Chem emissions driver that includes volcanic water vapor emissions that are specified by the user. This code adds these emissions to the ambient water vapor mass within the model environment. Van Eaton et al. (2012) demonstrated that the sticking efficiency of volcanic ash particles follow exponential curves. Using these fitted curves, the sticking efficiency coefficient, α, between two particles i and j may be calculated using a fitting coefficient, S. This coefficient varies with water vapor concentration, $[H_2O]$, and the radius of the colliding particles, r. A lookup table was added to select sticking coefficients based on this work by utilizing the water vapor content of the model cell and the particle size (Eq. (7) and Table 2). Importantly, this equation is computationally inexpensive to solve. Although electrostatic interactions are significant enough to cause aggregation of particles, they are most likely insignificant when compared to aggregation in the presence of water (James et al., 2003; Schumacher and Schmincke, 1995). Since the modeled background water rarely approaches 0% relative humidity, dry interactions are not parameterized in this study.

$$\alpha(ij, [H_2O]) = e^{-Sr} \quad (7)$$

Deleted: 3

The four aggregation equations (Eq. 2 to Eq. 5) are solved for volcanic ash bins 2 to 10 (Table 3) at every time step, for every model grid cell, and account for interaction of particles between the different bins by using the total mass to calculate

Deleted: ¶

the available number of primary particles available for aggregation. Large particles, greater than 1 mm in diameter, are included in WRF-Chem volcanic ash bin 1, which has been designated as the "aggregate" bin. All aggregates generated by the code are moved to bin 1 and their corresponding masses are subtracted from bins 2-10. The large particles (in bin 1) assume high fall velocities and contribute to ash fallout within periods of minutes (Rose and Durant, 2011). All volcanic ash removed from the model domain is stored in the ASH_FALL variable, allowing the analysis of fallout mass and location.

3. Case Study and Methods

The 2010 eruption of Eyjafjallajökull Volcano in Iceland has been selected to test the modified WRF-Chem modeling experiment. Eyjafjallajökull erupted in April and May 2010, dispersing ash over Europe that caused numerous flight delays over the course of weeks and a resulting loss of revenue to airlines in the billions of dollars (Harris et al., 2010). Due to Eyjafjallajökull's location and the availability of observational resources, it became one of the most studied and well-documented eruptions in history, providing numerous sources of data regarding the plumes characteristics. The German Aerospace Center (Deutsches Zentrum für Luft- und Raumfahrt, DLR) took several in situ measurements of Eyjafjallajökull's ash clouds over the course of the two months of eruptions by flying its Falcon aircraft into forecasted plume locations. Three of these flights are used for analysis in this study from 19 April, 16 May and 17 May. The flight paths corresponding to these flights are depicted using colored lines in Fig. 1. During the flights, Schumann et al. (2011) recorded particle number concentrations using a Grimm SKY-OPC 1.129 optical particle counter and a Particle Measuring Systems, Inc. (PMS) Forward Scattering Spectrometer Probe (FSSP), observing a range of particles from 0.25 and 24 μm. In addition, upper and lower mass concentration estimates were calculated using the minimum and maximum imaginary component of the refractive index, of which the FSSP was particularly sensitive. For the flight of May 17, a medium estimate of mass concentration was calculated. From these studies, information on particle number, mass concentration, plume heights and gas composition are available, providing one of the best in situ datasets available to study distal and proximal volcanic emissions (Schumann et al., 2011). In addition to these in situ data, Doppler radar measurements of the eruptive column and ground air sampling measurements were conducted by many groups to establish descriptive and accurate eruption source parameters (Arason et al., 2011; Devenish et al., 2012a, Devenish et al., 2012b; Stevenson et al., 2012). Observations of volcanic tephra fallout are also available and provide important insights into the PSD and transport of the distal Eyjafjallajökull ash clouds (Gudmundsson et al., 2012; Stevenson et al., 2012). In addition, volcanic ash aggregation was directly observed via high speed photography near the vent, lending proof that particle aggregation occurred in the plumes Eyjafjallajökull produced (Taddeucci et al., 2011).

3.1. Eyjafjallajökull Model Domain Setup

The newly implemented aggregation code was applied to the April and May 2010 eruptions of Eyjafjallajökull. Additionally, sensitivity studies were conducted using a hypothetic single eruption of Eyjafjallajökull on May 5th, 2010. In all studies, the model domain was centered at 50°N, 0°W, offsetting the Eyjafjallajökull vent (63.62°N, 19.61°E) to the

northwest of the domain to account for the predominant southwest trajectory of the ash clouds. The model was setup with a resolution of 10 km^2 per grid cell, and a total of 500 x 500 horizontal grid cells. This resolution was chosen as a compromise between the long time scale of the model study (on the order of months), the large spatial extent of the model domain required to study the physics of the distal plume, and the amount of available computational time. The domain is shown in Fig. 1 with Eyjafjallajökull marked in red. The model included 48 vertical pressure levels with the top level of the model set to 2,000 Pa. The integration time step of the dynamics and chemical fields was set to 30 seconds.

Meteorological fields were obtained from the National Center for Environmental Prediction Final Global Operational Analysis (NCEP FNL) datasets, ds083.2, accessed through the National Center for Atmospheric Research Data Archive (NCAR, 2000). These datasets represent the final analysis of historical Global Forecast System (GFS) model output. Ingest was conducted similar to Hirtl et al. (2019), using a 9 day spin up time before the first eruption on 14 April and with meteorological initializations every 48 hours. Each reinitialization of the meteorological fields required the model to idle for varying periods due to competing jobs in the supercomputer's scheduler queue. The 48 hour reinitialization of the meteorological fields balanced the need for sufficient synoptic scale time coverage and the extensive size (order of months) of the time domain. The WRF-Chem volcanic package was enabled with chemistry option 402, which includes ten particle sizes of volcanic ash (Stuefer et al., 2013). These particle sizes are shown in Table 3. The Yonsei University Planetary Boundary Layer (YSU PBL) scheme and the Noah Land Surface Model (LSM) were included for PBL and near ground physics (Chen and Dudhia, 2001; Hong et al., 2006).

Water was added to the model domain by multiplying the water content of Eyjafjallajökull's magma, 1.8% (Keiding and Sigmarsson, 2012) to the total erupted mass of 400 Tg for fine and coarse ash estimated by Taddeucci et al. (2011). This 1.8% multiplier produces water vapor emissions that agree with constraints constructed by comparing H_2O/SO_2 emission ratios using values from Allard et al. (2011), yielding a ratio of 458 mol/mol, and SO_2 emission rates from two remote sensing studies by Boichu et al (2013 and Thomas and Prata (2011). The code was modified to read in volcanic water vapor emissions rates into WRF-Chem as a callable Fortran module.

In addition, Hirtl et al. (2019) noted that the model topography of Eyjafjallajökull is smoothed at the 10 km^2 model spatial resolution, resulting in a vent height 400 m lower than the actual height of 1000 m. A 400-m height offset was applied to correct this.

3.2. Sensitivity Study Model Setup

Multiple sensitivity studies were conducted in order to assess: 1) the overall change in mass due to aggregation, 2) the effects of different fractal dimensions, D_f, on the aggregation rate, 3) the contribution of each collision kernel, A_B, A_S and A_{DS}, to the decrease in domain ash mass and 4) the effect of adding coupled water vapor emissions to the model domain on the aggregation rate. A list of these sensitivity studies, including the parameters varied and the analysis approach used, is presented in Table 4. These sensitivity studies were conducted on a smaller time slice of the parent domain, using a 9 hour

Deleted: for high spatial resolution simulations at

Deleted: with

Commented [SDE3]: Reviewer one and two both asked that we clarify why we chose a 10 km2 model domain. This is one part of the explanation. The second part is detailed in the conclusions when we suggest that further studies could contain a nested domain over the vent.

Commented [SDE4]: We try to explain, here, why the 48 hour model reinitialization was chosen. It was a constraint placed by the availability of computational time. We also reference Hirtl et al (2019) who utilized a similar approach.

Commented [SDE5]: Reviewer two requested a table listing the different sensitivity studies included.

eruptive event on May 5th, 2019, initialized at 00:00Z with a rate of 4 x 10^6 kg s^{-1}, which corresponds to an average value of Eyjafjallajökull's largest eruptions. A 72 hour spin up time was included prior to the eruption initialization to allow the meteorological fields to stabilize, and was then run for 6 days, ending 00:00Z on the 11th of May. The smaller model time domain allowed for new meteorological fields to be reinitialized every 24 hours, as opposed to 48 hours in the longer timescale study. Each volcanic ash bin was populated with 10% of the total erupted mass in order to simplify output analysis.

In order to assess how the aggregation code affects model output, WRF-Chem was run with and without the aggregation code enabled. Due to a lack of experimental data, a choice of fractal dimension, D_f, is difficult. Therefore, the fractal dimension, D_f, was varied to measure its effects on the overall aggregation rate. The span of fractal dimensions chosen ranges from $D_f = \{2.5, 2.6, 2.7, 2.8, 2.9, 2.95, 2.98, 2.99, 3.0\}$ and is based on studies by Costa et al. (2010) and from a similar study of Mount Saint Helens and Mount Spurr using Fall3D by Folch et al. (2010).

The contribution of each collision kernel, A_B, A_S and A_{DS}, to the total reduction in domain mass was also assessed by using the same domain and eruption parameters, and enabling only one kernel at a time using a fractal dimension of 2.5 and 3.0. The total change in mass from each kernel was then divided by the total change in mass with all kernels enabled to find the percent contribution.

The impacts of the inclusion of water vapor on the aggregation rate were studied by running the code with and without the 1.8% water vapor emissions included in the model domain. For the simulation run without water vapor emissions, only background water vapor from the FNL datasets were used.

3.3 Model Setup for April and May 2010 Eruptions of Eyjafjallajökull

WRF-Chem was also configured to simulate Phase I (April 14-18, 2010) and the Phase III (May 4-18 2010) eruptions of Eyjafjallajökull using the same model domain described above. Phase II eruptions were effusive rather than explosive and ejected tephra at much lower altitudes of 2 to 4 km ASL (Gudmundsson et al., 2012) and were thus not included in this modeling case study.

Eruption source parameters (ESP) for Eyjafjallajökull were adapted from Mastin et al. (2014) and Hirtl et a. (2019). Camera footage and C-band Doppler radar measurements were used to establish three hourly plume heights for the April and May 2010 eruptions (Arason et al., 2011; Mastin et al., 2009; Hirtl et al., 2019). These plume heights were used to calculate eruption rates based on the plume height/eruption rate relationship derived by Mastin et al. (2009). The total erupted mass was then scaled based on work by Gudmundsson et al. (2012) such that the total ash mass ejected over the eruptive phases agreed with the 170 Tg Phase I estimate and 190 Tg Phase III estimates for fine ash stated (Hirtl et al., 2019). The bimodal, silicic (S2) ESP particle size distribution (Table 3) was used to populate the ten volcanic ash bins in the model (Mastin et al., 2009). The three hourly plume heights and eruption rates used in the study are presented in Fig. 2.

In this study, all aggregation collision kernels were enabled, and water vapor emissions as described previously were added to the model domain at each time step. As mentioned earlier, the choice of a fractal dimension is hindered by a

Deleted: N

Deleted: were ingested

Deleted: for high fidelity

Commented [SDE6]: In reply to reviewer two who asked why we switched to 24 hour reinitializations here.

Deleted: .3

lack of experimental data. Folch et al. (2010) conducted linear regression analysis of repeated model run comparisons to tephra fallout measurements from eruptions originating at Mount Spurr and Mount Saint Helens. This study resulted in the use of a D_f = 2.99 fractal dimension. Due to a lack of experimental data on the development of volcanic ash fractal dimensions, and the fact that aggregate fractal dimensions are not necessarily constant with time, D_f was set at the upper bound of 3.0, providing a maximum effect of particle aggregation.

Commented [SDE7]: Reviewer two asked if a fractal dimension of 3 is realistic. As I mentioned in my reply, it is because 1) Folch et al. note this in the cited work for 2.99 and 2) because in the sensitivity study to follow, a fractal dimension of 2.99 varies only very slightly from 3.0.

4. Results

The newly implemented aggregation parameterization was first assessed with a sensitivity study of a singular eruptive event, and then by application to the entire Phase I and Phase III eruption periods.

4.1. Sensitivity Study Results

Varying the fractal dimension between 2.5 and 3.0 resulted in a range of aggregation rates. Figure 3 illustrates the change in domain mass from a single 9-hour eruption on May 5th at 00:00Z with a constant eruption rate of 4 x 10^6 kg s^{-1}. As expected, higher values of D_f result in higher rates of aggregation with the largest jumps in the aggregation rate between D_f = 3.0 and 2.8. The degree to which aggregation reduced the overall ash domain mass can be seen in the peak mass loadings at hour 9 in Fig. 3. Here, the peak domain mass using D_f = 3.0 is 17.4 Tg. This is 72% reduction in peak mass compared to the non-aggregation enabled run of 62.9 Tg. Lower values of D_f provide almost no change in the total domain mass. For example, D_f = 2.5 results in a 0.7 % decrease in peak mass by about 0.5 Tg.

To quantify the change in aggregation rate, volcanic ash lifetimes in terms of e-folding were calculated. This analysis is presented in Fig. 4 and indicates a range of e-folding times from 72 hours with no aggregation code enabled to 15 hours with maximum aggregation considered (D_f = 3.0). As the fractal dimension increases, the atmospheric lifetime of volcanic ash decreases due to the incorporation of more volcanic ash particles into each aggregate. When considering fractal dimensions 2.7 and lower, the total lifetime is reduced only slightly, less than 4%. Larger decreases in lifetime become apparent with D_f = 2.8 (10% decrease) and jump thereafter to a maximum 79.5% decrease at D_f = 2.99 and D_f = 3.0 (same decrease for both). Based on work by Folch et al. (2019), it is assumed that an optimal value of the fractal dimension likely lies near D_f = 2.99, which corresponds to a 79.5% difference in e-folding times. In terms of volcanic ash lifetime, on hourly timescales, there is no difference between D_f = 3.0 and 2.99.

Deleted: g

Commented [SDE8]: Reviewer one requested that we consider a sensitivity study of the extent to which the plume travelled. The study of atmospheric residency time is exactly that, and is presented starting here.

Figure 5 shows the extent to which each kernel contributed to the overall change in the model domain's ash mass by enabling each kernel independently. Two fractal dimensions were considered, D_f = 2.5 and 3.0, and both affected each kernel's contribution to aggregation differently. The differential sedimentation kernel, A_{DS}, for example contributed to the majority of the change in domain mass over the course of the 96-hour model run (≈ 99%) when D_f was set to 3.0, but contributed only 5% on average with D_f = 2.5. The Brownian kernel became the major contributor to aggregation in the case

of D_f = 2.5, contributing to over 90% of the aggregation. This agrees with parametric studies of varying fractal dimensions by Costa et al. (2010), who noted this trade between A_{DS} and A_B when considering fine ash particles (<63 μm). Overall, fluid shear interactions were the minor contributor to aggregation for both fractal dimensions. While its contribution to aggregation approaches that of A_{DS} for D_f = 2.5, it is many orders of magnitude lower than A_B or A_{DS} for D_f = 3.0. Figure 6 illustrates the total domain mass for fine ash (bins 7-10) in panel (a) as well as their percentage of total domain mass in panel (b), representing the PSD of the fine ash fraction. Figure 6 considers maximum aggregation with D_f = 3.0. The bins with larger ash particles (1-6) were not included due to the rapid decrease in their domain mass as a result of their high settling velocities. Figure 6 (a) depicts a decreased mass loading for each bin when aggregation is enabled, as well as a shorter lifetime, as expected. Figure 6 (b) depicts a shift in the particle size distribution due to aggregation. The aggregation code results in less contribution from fine ash particles (bins 7, 8 and 9), resulting in a shift of the PSD towards bin 10. Bin 10 in the aggregation enabled code makes up an extra 10% of the model domain mass upon reaching near steady state at model hour 120. This is the result of the increased aggregation of the larger sizes particles since larger radii result in a larger probability cross section of collision and subsequent aggregate formation.

Coupling water emissions resulted in a very small increase in aggregation rate, lowering the total domain mass on the order of Mg hr^{-1}, much lower than the overall loss rate of ash due to aggregation on the order of Tg hr^{-1} (6 orders of magnitude). The sticking efficiency, Eq. (6), is high (> 90%) for small particles (< 63 μm). As the residence time of large particles is very short, the sticking efficiency is applicable to the narrow range of particle sizes that persist in the domain (Bins 7-10, < 32.5 μm). These particle sizes correspond to a narrow range of sticking efficiencies (.87 to .97), regardless of the water vapor concentration.

4.2. Eyjafjallajökull Study Results

The ash cloud dynamics generated by WRF-Chem over the model period agree with other modeling studies of Eyjafjallajökull utilizing WRF-Chem (Hirtl et al., 2019; Webley et al., 2012). Figure 7 provides an example of the output from WRF-Chem for April 15 and 16, 2010. The dynamics of the ash clouds are apparent. The plume moves south and east towards the coasts of Scandinavia and northern Europe then splits into two plumes: one residing over Sweden and Finland and the other passing through multiple northern European countries.

Model output also agrees with airborne in situ measurements. The DLR research aircraft conducted 13 flights on 11 different days that transected Eyjafjallajökull's ash clouds over the course of the Phase I and Phase III eruptions (Schumann et al., 2011). Predicted ash concentrations from WRF-Chem were compared to the in situ observational data from three of these flights: April 19 and May 16, and 17, 2010. WRF-Chem volcanic ash bins 8, 9 and 10 correspond to the particle size detection limits of the Grimm OPC and PMS FSSP aboard the Falcon aircraft and were thus chosen for comparisons.

Figure 8 presents time series plots of WRF-Chem output and DLR measurements. Figures 8(a), 8(c), and 8(e) show the WRF-Chem output in mass concentration (g m^{-3}). Figures 8(b), 8(d) and 8(f) show the WRF-Chem ash bin as number

Deleted: ¶

Deleted: 3.9

Deleted: cast

Deleted: cast

concentrations by using an assumed particle density of 2500 kg m^{-3} (Brown et al., 2012) in order to make direct comparisons to the Grimm OPC and FSSP detectors.

Temporal changes in observed and modelled ash concentrations agreed moderately well for the April 19 flight (Fig. 8a and 8b). Analysis of particle number densities in Fig. 8 (b) for April 14 shows 5 significant overestimations of volcanic ash by the non-aggregation enabled code, between 50-75% at 14:55 and 15:07, between 15:15-15:18, between 15:35-15:42 and between 16:55-17:06. These overestimations did not occur when the aggregation code was used. One peak concentration was observed at 15:30 UTC on April 19, which was not resolved by WRF-Chem (Fig. 8b). An analysis of the surrounding grid cells in the vertical and horizontal did not contain this peak, however the next vertical grid cell in the positive k contained higher ash concentrations (similar order of magnitude). This analysis, along with analysis of the integrated volcanic ash over the time span of the peak, lead to the conclusion that this lack of peak concentration in the model is a result of model diffusion, which is typical for all Eulerian models. Smaller domain grid cells permit better comparison with point observations, but decreases in grid cell sizes are computationally expensive and in many cases impossible to resolve completely.

Number density readings for May 15 (Fig. 8d) contained more robust data than mass concentration (Fig. 8c) and was therefore used in the analysis. Here, a large overestimation of ash is calculated by WRF-Chem when not using the aggregation code. A peak of 290 particles cm^{-3} are observed in the unmodified code, almost 10 times higher than observed. With aggregation enabled, the WRF-Chem solution is much closer to the observed numbers at a maximum of 45 particles cm^{-3}.

On May 17 (Fig. 8e and 8f), the aircraft performed a steep transect through a plume with larger ash particles. Almost no ash concentration was recorded at the lowest flight altitude reached during the middle of the flight at 16:40 UTC. At this same time, WRF-Chem predicted concentrations in excess of 400 g m^{-3}. Where the plume locations do agree, there is improved agreement between the aggregation enabled code and the airborne observations of mass concentration. For the entire time range, observations where the aggregation code produced mass readings in the same order of magnitude as those observed by DLR were counted. This total was then divided by the total flight time and resulted in an average 80% agreement of the data (78% for April 19, 78% for May 15 and 83% for May 17). This fell to an average of 62% when the code was run without aggregation, using the same methodology.

In addition to comparisons with Schumann et al. (2011) in situ measurements, WRF-Chem tephra fallout was also compared to field measurements of tephra collected by Stevenson et al., (2012) in the United Kingdom (UK). Figure 9 depicts the mass of tephra deposited in the model domain from all April 2010 eruptions in panel (a) and from May 2010 eruptions in panel (b). Stevenson et al. (2012) report three sampling periods that overlap with the model domain times in this study. For example, Stevenson et al. (2012) counted 218 grains of tephra per cm^2, at Benbecula in the Outer Hebrides (57.43N, 7.34W, Fig. 9(a), white circle), with a mean diameter of 18 $\pm$ 7 μm while sampling between 13-20 May, 2010. Assuming an average density of 2,500 kg m^{-3} yields a tephra concentration between 20 and 45 mg m^{-2}, compared to 31 mg m^{-2} predicted by WRF-Chem with the aggregation code enabled during the same time range. Samples taken at Leicestershire (52.73°N, 1.16°W, Fig. 9(b), white circle) between 25 April and 3 May, 2010 estimate a range of tephra mass on the ground

Deleted: Typical of any Eulerian air quality model, WRF-Chem tends to diffuse ash concentrations, an effect that is also dependent on the model resolution.

Formatted: Font: (Default) +Headings (Times New Roman), 10 pt

Formatted: Font: (Default) +Headings (Times New Roman), 10 pt

Deleted: the

Formatted: Font: (Default) +Headings (Times New Roman), 10 pt

Commented [SDE9]: We add text here to help Reviewers 1 and 2 understand why this peak was not resolved by WRF. It is a result of the diffusion inherent in gridded moels.

Deleted: 9C

Formatted: Font: (Default) +Headings (Times New Roman)

Formatted: Font: (Default) +Headings (Times New Roman)

between 51 and 119 mg m^{-2}, also near the WRF-Chem estimate of 41 mg m^{-2} (80% of observed mass) between those dates. Another sample from Lincolnshire (52.74N, 0.38W, Fig. 9(b), white circle) covered a period from 24-30 April 2010. In this case, tephra fallout between 3 and 13 mg m^{-2} were measured, whereas WRF-Chem predicted a smaller value of 1.2 mg m^{-2} (40% of observed mass). The smaller estimates for the Lincolnshire and Leicestershire sites may be explained by the lack of model data covering April 27 –May 3, as the last modeled hour was 00:00 UTC on April 27. When considering WRF-Chem run without aggregation, the modeled fallout seen in these areas is minimal, with less than 1 mg m^{-2} observed.

The aggregation code altered the total domain mass of each volcanic ash bin. To study this change, the model domain mass was analyzed from May 14 to 18, 2010. This time frame represents the last 96 hours of modeled eruptions and includes a high degree of variability in the eruption rate and plume height (see Fig. 2). The total domain mass is presented in Fig. 10 without (a) and with (c) the aggregation code enabled. To analyze the PSD, the mass of each volcanic ash bin was divided by the total model domain mass. The resulting percentages are presented in Fig. 10(b) and 10(d). The top panels, Fig. 10(a) and 10(b), depict WRF-Chem output without the use of the aggregation code, whereas the lower panels, Fig. 10(c) and 10(d), include the aggregation code. The short atmospheric lifetime of the large particles in bins 1-3 result in small masses during this time frame compared to bins 4-10 including smaller particle sizes. As such, only bins 4-10 are depicted in Fig. 10. Major changes in the eruption rates are annotated on the time axis with red marks.

Deleted: 1

Two important observations are noted when aggregation is included. First, the total domain mass in each bin is reduced and second, the PSD shifts towards smaller sized particles during eruptive events. For example, the initial period in Fig. 10 is eruptive until the first red mark on the 14th at 09:00UTC. During this period, the eruption rate is 7.36 x10^5 kg s^{-1} (7.949 Tg per 3 hours). In the non-aggregation enabled code, the dominant ash species are bins 6, 7 and 8 which have peak masses of 3.7, 4.1 and 3.3 Tg, respectively. In the non-aggregation enabled code, bins 6, 7 and 8 make up the majority of the domain as mass, contributing 21.5%, 24.1% and 19.3% of the total domain mass. When the aggregation code is enabled, the total domain mass for each of the bins is reduced to 1.0, 1.5 and 1.4 Tg, respectively, which is around one third of the original peak mass, showing an overall reduction. Additionally, their contribution to the overall domain mass changes to 14.6%, 21.1% and 20.5%. The smaller bin 8 ends up with more of the mass, with the other two contributing less to the PSD. In fact, the smaller bins 9 and 10 also contribute more to the overall domain mass, increasing from a peak of 13.1% and 9.6% on the 14th and 09:00UTC without the aggregation code enabled to 15.2% and 11.6% with the aggregation code enabled. Overall there is a slight shift towards smaller particle bins during eruptive events.

Interestingly, this trend in the PSD is not observed during periods of decreased eruption rates, while trends in overall domain mass continue are still observed. Between marks 1 and 2, the eruption rate decreases from 7.36 x 10^5 kg s^{-1} to 1.09 x 10^5 kg s^{-1}. During this period of slower eruption rates, the total domain mass continues to increase, however it is much lower when aggregation is considered. The PSD, on the other hand, remains consistent, with bins 8, 9 and 10 trending similarly in the non-aggregation and aggregation enabled case. This suggests that the aggregation code is most effective during eruptive events when particles are in high concentration.

Without aggregation, the only sinks for volcanic ash are via settling, which is dependent on gravity and water vapor concentration, or via the plume traveling out of the model domain. For finer ash particles, removal via settling is minimal when compared to larger particles which is evident in Fig. 10(a) and 10(c). During periods of less volatile eruptions, such as between markers 1 and 2 or markers 3 and 4, the fine ash bins reach a steady state where the source of ash is almost equal to the sink, i.e. settling. This is evident in the horizontal slope of the bin domain mass. This is not true for larger particles whose settling velocities are high enough to remove them faster than they are added. Aggregation adds an additional sink that is noticed subtly during less eruptive phases as the slight dips in domain mass, as well as the more pronounced decreases in the slope of the change in domain mass during periods of higher eruption rates.

Commented [SDE10]: Reviewers 1 and 2 wanted clarification that WRF does incorporated the effects of water vapor on settling. We've added some text here to clarify this.

Deleted: Without aggregation, the only sinks for volcanic ash are via settling or via the plume traveling out of the model domain.

6. Summary and Conclusions

A parameterization of volcanic ash particle aggregation has been implemented into the fully coupled WRF-Chem model. The new model has been tested for ash loadings and lifetimes. A simplified version of the Smoluchowski coagulation equation (Costa et al., 2010; Dekkers and Friedlander, 2002; Folch et al., 2010, 2016; Smoluchowski, 1917) was incorporated into the WRF-Chem model. This simplified method was chosen for its computational efficiency, allowing the aggregation rate to be calculated at each model time step in line with the atmospheric dynamics.

The effects of the aggregation code were assessed by applying it to a high-resolution model study of the 2010 eruptions of Eyjafjallajökull, including a single study of a 9 hour test eruption. The effect of each particle collision kernel on the overall aggregation rate (Eq. 2) was studied. The degree to which each kernel affected aggregation depended on the choice of the fractal dimension, D_f. The differential sedimentation kernel provided the largest contribution by orders of magnitude when a fractal dimension of 3.0 was chosen, however the Brownian kernel dominated when a fractal dimension of 2.5 was chosen. This result suggests that vertical motion, when a fractal dimension near 3.0 is chosen, is the primary driving force behind particle interactions in the aggregation process, rather than random (Brownian) or horizontal (shear) motions. Additionally, analysis of the volcanic ash lifetime shows that varying the fractal dimension may greatly vary the lifetime, especially when considering fractal dimensions between 3.0 and 2.8.

Commented [SDE11]: Reviewer asked what the implications for the different processes being dominant are. They are mentioned here. Primarily that vertical motion is the primary driver of aggregation.

The Eyjafjallajökull model study was assessed by comparison to aircraft in situ measurements taken by DLR as well as tephra fallout samples measured in the United Kingdom. By comparing WRF-Chem calculated volcanic ash mass concentrations using the aggregation code to those observed by DLR, an average 80% match in an order of magnitude was observed for the 3 flights analyzed. Additionally, non-aggregation enabled code calculated 20-50% higher volcanic ash concentrations on numerous occasions, where the aggregation enabled code did not. The aggregation enabled WRF-Chem code tended not to overestimate volcanic ash, or to overestimate less than the non-aggregation enabled version, potentially yielding more realistic ash concentrations which may benefit aircraft hazard mitigation forecasting.

As the plume transported over the United Kingdom, WRF-Chem predicted ash fallout that compared well to field measurements. Tephra fallout generated by WRF-Chem fell within observed values at one sample location, and predicted on

Deleted:

average 60% of the fallout at two others. This suggests that WRF-Chem may be used to model not only the atmospheric transport of ash clouds, but the deposition of ash as well.

Importantly, these observations all suggest that two factors drive volcanic ash aggregation when including aggregation in the WRF-Chem code. First, volcanic ash concentration is noted to be the primary driving factor behind aggregation rate. The majority of model domain mass decreased near the vent where concentrations of ash are high. In addition, PSD analysis indicates that bins with higher portions of the eruption PSD undergo faster rates of ash aggregation. Bins with a larger share of the eruption PSD will aggregate faster due to their increased probability of collision. Second, vertical motions of ash falling through the atmosphere also drive the aggregation process through differential sedimentation for realistic ranges of fractal dimension (between 2.95 and 3.0).

The inclusion of this aggregation scheme into WRF-Chem provides research and operational meteorological communities a second VATD model to Fall3D that includes volcanic ash aggregation and is the first to run aggregation in an inline fashion where aggregation equations are solved at each model time step (Folch et al., 2010). This inline computation of volcanic ash yields many benefits. For example, the code identifies the driving forces behind volcanic ash aggregation, i.e. ash concentration and differential sedimentation rates, and allows for the study of the effects of water vapor concentration on the aggregation rate. In addition, it allows the study of changes in particle size distributions due to enhanced ash settling as a result of aggregation processes, which are of particular importance to remote sensing communities where the effective particle size directly impacts the spectral methods used for detection. While this study focused primarily on the distal ash cloud transport and aggregation physics, the calculations integrated into WRF would also benefit a higher resolution, nested domain over the emission source to study proximal aggregation effects. The modified code also benefits the operational volcanic ash modeling community by providing model derived ash mass concentrations that augment existing VATD models for use in aircraft hazard mitigation. In the operational setting, first guess, expedient model output from VATD models can be augmented by WRF derived mass loadings as they become available. The time requirement for this is feasible in the operational setting as the modified code is computationally expedient. It ingests output from global models, such as ECMWF and GFS, and runs volcanic ash dispersion and aggregation code while simultaneously calculating mesoscale atmospheric dynamics, eliminating the need for additional, offline calculations. Additionally, this code results in another model that provides researchers a robust treatment of ash microphysical processes as they are erupted, transported and removed from a model domain. Ultimately, this study provides another step towards the inclusion of volcanic ash aggregation, an important physical process, into VATD models.

Commented [SDE12]: This, in addition to earlier comments, helps point out that these equations can be used in studies of the proximal plume using a higher resolution.

Deleted: another

Deleted: Additionally,

Deleted: dispersion runs

Commented [SDE13]: The discussion here has been updated to explain why the use of WRF is potentially important to operational forecasting. This stems from a comment by reviewer 2.

7. Acknowledgements

This publication is the result of research sponsored in part by the NOAA Cooperative Institute for Alaska Research (CIFAR) with funds from NOAA under cooperative agreement NA13OAR4320056 with the University of Alaska Fairbanks (UAF). The Alaska Space Grant Program supported this work. Computational time was provided by UAF Research Computing Systems at the Geophysical Institute and the Department of Defense High Performance

Computing and Modernization Program. We acknowledge our colleague Dr. Alexa Van Eaton for the fruitful discussions throughout this research.

505

References

Allard, P., Burton, M., Oskarsson, N., Michel, A. and Polacci, M.: Magmatic gas composition and fluxes during the 2010 Eyjafjallajökull explosive eruption: implications for degassing magma volumes and volatile sources, in Geophys. Res. Abstr, vol. 13., 2011.

Angell, J. K.: Comparison of stratospheric warming following Agung, El Chichon and Pinatubo volcanic eruptions, Geophys. Res. Lett., 20(8), 715–718, 1993.

Arason, P., Petersen, G. N. and Bjornsson, H.: Observations of the altitude of the volcanic plume during the eruption of Eyjafjallajökull, April–May 2010, Earth Syst. Sci. Data, 3(1), 9–17, doi:10.5194/essd-3-9-2011, 2011.

Boichu, M., Menut, L., Khvorostyanov, D., Clarisse, L., Clerbaux, C., Turquety, S. and Coheur, P.-F.: Inverting for volcanic SO2 flux at high temporal resolution using spaceborne plume imagery and chemistry-transport modelling: the 2010 Eyjafjallajökull eruption case-study, Atmospheric Chem. Phys., 13(17), 8569–8584, doi:10.5194/acp-13-8569-2013, 2013.

Bonadonna, C., Genco, R., Gouhier, M., Pistolesi, M., Cioni, R., Alfano, F., Hoskuldsson, A. and Ripepe, M.: Tephra sedimentation during the 2010 Eyjafjallajökull eruption (Iceland) from deposit, radar, and satellite observations, J. Geophys. Res. Solid Earth, 116(B12), B12202, doi:10.1029/2011JB008462, 2011.

Booth, B. and Walker, G. P. L.: Ash Deposits from the New Explosion Crater, Etna 1971, Philos. Trans. R. Soc. Lond. Math. Phys. Eng. Sci., 274(1238), 147–151, doi:10.1098/rsta.1973.0034, 1973.

Brown, R. J., Bonadonna, C. and Durant, A. J.: A review of volcanic ash aggregation, Phys. Chem. Earth Parts ABC, 45–46, 65–78, doi:10.1016/j.pce.2011.11.001, 2012.

Carey, S. N. and Sigurdsson, H.: Influence of particle aggregation on deposition of distal tephra from the May 18, 1980, eruption of Mount St. Helens volcano, J. Geophys. Res. Solid Earth, 87(B8), 7061–7072, doi:10.1029/JB087iB08p07061, 1982.

Casadevall, T. J.: The 1989–1990 eruption of Redoubt Volcano, Alaska: impacts on aircraft operations, J. Volcanol. Geotherm. Res., 62(1–4), 301–316, doi:10.1016/0377-0273(94)90038-8, 1994.

Chen, F. and Dudhia, J.: Coupling an Advanced Land Surface–Hydrology Model with the Penn State–NCAR MM5 Modeling System. Part I: Model Implementation and Sensitivity, Mon. Weather Rev., 129(4), 569–585, doi:10.1175/1520-0493(2001)129<0569:CAALSH>2.0.CO;2, 2001.

Chin, M., Rood, R. B., Lin, S.-J., Müller, J.-F. and Thompson, A. M.: Atmospheric sulfur cycle simulated in the global model GOCART: Model description and global properties, J. Geophys. Res., 105(D20), 24671–24,687, doi:10.1029/2000JD900384, 2000.

Cole-Dai, J.: Volcanoes and climate, Wiley Interdiscip. Rev. Clim. Change, 1(6), 824–839, doi:10.1002/wcc.76, 2010.

Cornell, W., Carey, S. and Sigurdsson, H.: Computer simulation of transport and deposition of the campanian Y-5 ash, J. Volcanol. Geotherm. Res., 17(1–4), 89–109, doi:10.1016/0377-0273(83)90063-X, 1983.

Costa, A., Folch, A. and Macedonio, G.: A model for wet aggregation of ash particles in volcanic plumes and clouds: 1. Theoretical formulation, J. Geophys. Res. Solid Earth, 115(B9), B09201, doi:10.1029/2009JB007175, 2010.

Dekkers, P. J. and Friedlander, S. K.: The Self-Preserving Size Distribution Theory: I. Effects of the Knudsen Number on Aerosol Agglomerate Growth, J. Colloid Interface Sci., 248(2), 295–305, doi:10.1006/jcis.2002.8212, 2002.

Devenish, B. J., Thomson, D. J., Marenco, F., Leadbetter, S. J., Ricketts, H. and Dacre, H. F.: A study of the arrival over the United Kingdom in April 2010 of the Eyjafjallajökull ash cloud using ground-based lidar and numerical simulations, Atmos. Environ., 48, 152–164, doi:10.1016/j.atmosenv.2011.06.033, 2012a.

Devenish, B. J., Francis, P. N., Johnson, B. T., Sparks, R. S. J. and Thomson, D. J.: Sensitivity analysis of dispersion modeling of volcanic ash from Eyjafjallajökull in May 2010, J. Geophys. Res. Atmospheres, 117(D20) [online] Available from: http://onlinelibrary.wiley.com/doi/10.1029/2011JD016782/full (Accessed 25 April 2016b), 2012.

Folch, A., Costa, A. and Macedonio, G.: FALL3D: A computational model for transport and deposition of volcanic ash, Comput. Geosci., 35(6), 1334–1342, doi:10.1016/j.cageo.2008.08.008, 2009.

Folch, A., Costa, A., Durant, A. and Macedonio, G.: A model for wet aggregation of ash particles in volcanic plumes and clouds: 2. Model application, J. Geophys. Res. Solid Earth, 115(B9), B09202, doi:10.1029/2009JB007176, 2010.

Folch, A., Costa, A. and Macedonio, G.: FPLUME-1.0: An integrated volcanic plume model accounting for ash aggregation, Geosci. Model Dev. Discuss., 8(9), 8009–8062, doi:10.5194/gmd-9-431-2016, 2016.

Gilbert, J. S. and Lane, S. J.: The origin of accretionary lapilli, Bull. Volcanol., 56(5), 398–411, doi:10.1007/BF00326465, 1994.

Gudmundsson, M. T., Thordarson, T., Höskuldsson, Á., Larsen, G., Björnsson, H., Prata, F. J., Oddsson, B., Magnússon, E., Högnadóttir, T., Petersen, G. N., Hayward, C. L., Stevenson, J. A. and Jónsdóttir, I.: Ash generation and distribution from the April-May 2010 eruption of Eyjafjallajökull, Iceland, Sci. Rep., 2, 572, doi:10.1038/srep00572, 2012.

Harris, A. J. L., Gurioli, L., Hughes, E. E. and Lagreulet, S.: Impact of the Eyjafjallajökull ash cloud: A newspaper perspective: Impact of the Eyjafjallajökull Ash Cloud, J. Geophys. Res. Solid Earth, 117(B9), doi:10.1029/2011JB008735, 2012.

Hirtl, M., Stuefer, M., Arnold, D., Grell, G., Maurer, C., Natali, S., Scherllin-Pirscher, B. and Webley, P.: The effects of simulating volcanic aerosol radiative feedbacks with WRF-Chem during the Eyjafjallajökull eruption, April and May 2010, Atmos. Environ., 198, 194–206, doi:10.1016/j.atmosenv.2018.10.058, 2019.

Hong, S.-Y., Noh, Y. and Dudhia, J.: A New Vertical Diffusion Package with an Explicit Treatment of Entrainment Processes, Mon. Weather Rev., 134(9), 2318–2341, doi:10.1175/MWR3199.1, 2006.

Jacobson, M. Z.: Fundamentals of atmospheric modeling, 2nd ed., Cambridge university press., 2005.

James, M. R., Lane, S. J. and Gilbert, J. S.: Density, construction, and drag coefficient of electrostatic volcanic ash aggregates, J. Geophys. Res. Solid Earth 1978–2012, 108(B9), doi:10.1029/2002JB002011, 2003.

Jullien, R. and Botet, R.: Aggregation and fractal aggregates, Ann Telecomm, 41, 343, 1987.

Keiding, J. K. and Sigmarsson, O.: Geothermobarometry of the 2010 Eyjafjallajökull eruption: New constraints on Icelandic magma plumbing systems, J. Geophys. Res. Solid Earth, 117(B9), doi:10.1029/2011JB008829, 2012.

Kristiansen, N. I., Stohl, A., Prata, A. J., Bukowiecki, N., Dacre, H., Eckhardt, S., Henne, S., Hort, M. C., Johnson, B. T., Marenco, F., Neininger, B., Reitebuch, O., Seibert, P., Thomson, D. J., Webster, H. N. and Weinzierl, B.: Performance

assessment of a volcanic ash transport model mini-ensemble used for inverse modeling of the 2010 Eyjafjallajökull eruption, J. Geophys. Res. Atmospheres, 117(D20), doi:10.1029/2011JD016844, 2012.

Lee, C. and Kramer, T. A.: Prediction of three-dimensional fractal dimensions using the two-dimensional properties of fractal aggregates, Adv. Colloid Interface Sci., 112(1–3), 49–57, doi:10.1016/j.cis.2004.07.001, 2004.

Lin, J., Brunner, D., Gerbig, C., Stohl, A., Luhar, A. and Webley, P.: Lagrangian Modeling of the Atmosphere, American Geophysical Union., 2012.

Mastin, L. G., Guffanti, M., Servranckx, R., Webley, P., Barsotti, S., Dean, K., Durant, A., Ewert, J. W., Neri, A., Rose, W. I., Schneider, D., Siebert, L., Stunder, B., Swanson, G., Tupper, A., Volentik, A. and Waythomas, C. F.: A multidisciplinary effort to assign realistic source parameters to models of volcanic ash-cloud transport and dispersion during eruptions, J. Volcanol. Geotherm. Res., 186(1–2), 10–21, doi:10.1016/j.jvolgeores.2009.01.008, 2009.

Mastin, L. G., Bonadonna, C., Folch, A., Stunder, B. J., Webley, P. W. and Pavolonis, M. J.: Summary of data on well-documented eruptions for validation of volcanic ash transport and dispersal models, VHub.org [online] Available from: https://vhub.org/resources/4044/download/summary_table_2016.06.11.htm (Accessed 19 September 2016), 2014.

Mazzocchi, M., Hansstein, F., Ragona, M. and others: The 2010 volcanic ash cloud and its financial impact on the European airline industry, in CESifo Forum, vol. 11, pp. 92–100, Ifo Institute for Economic Research at the University of Munich., 2010.

Miller, T. P. and Casadevall, T. J.: Volcanic ash hazards to aviation, Encycl. Volcanoes, 915–930, 2000.

NCAR: NCEP FNL Operational Model Global Tropospheric Analyses, continuing from July 1999, [online] Available from: https://rda.ucar.edu/datasets/ds083.2/ (Accessed 7 February 2019), 2000.

Peckham, S. E., Grell, G., McKeen, S., Barth, M., Pfister, G., Wiedinmyer, C., Fast, J. D., Gustafson, W. I., Zaveri, R. A., Easter, R. C. and others: WRF/Chem Version 3.9 User's Guide, US Department of Commerce, National Oceanic and Atmospheric Administration, Oceanic and Atmospheric Research Laboratories, Global Systems Division. [online] Available from: https://ruc.noaa.gov/wrf/wrf-chem/Users_guide.pdf, 2018.

Prata, A. J. and Prata, A. T.: Eyjafjallajökull volcanic ash concentrations determined using Spin Enhanced Visible and Infrared Imager measurements, J. Geophys. Res. Atmospheres 1984–2012, 117(D20), doi:10.1029/2011JD016800, 2012.

Rose, W. I. and Durant, A. J.: Fine ash content of explosive eruptions, J. Volcanol. Geotherm. Res., 186, 32–39, doi:10.1016/j.jvolgeores.2009.01.010, 2009.

Rose, W. I. and Durant, A. J.: Fate of volcanic ash: Aggregation and fallout, Geology, 39(9), 895–896, doi:10.1130/focus092011.1, 2011.

Schumacher, R. and Schmincke, H.-U.: Models for the origin of accretionary lapilli, Bull. Volcanol., 56(8), 626–639, doi:10.1007/BF00301467, 1995.

Schumann, U., Weinzierl, B., Reitebuch, O., Schlager, H., Minikin, A., Forster, C., Baumann, R., Sailer, T., Graf, K., Mannstein, H., Voigt, C., Rahm, S., Simmet, R., Scheibe, M., Lichtenstern, M., Stock, P., Ruba, H., Schauble, D., Tafferner, A., Rautenhaus, M., Gerz, T., Ziereis, H., Krautstrunk, M., Mallaun, C., Gayet, J. F., Lieke, K., Kandler, K., Ebert, M., Weinbruch, S., Stohl, A., Gasteiger, J., Gross, S., Freudenthaler, V., Wiegner, M., Ansmann, A., Tesche, M., Olafsson, H. and Sturm, K.: Airborne observations of the Eyjafjalla volcano ash cloud over Europe during air space closure in April and May 2010, Atmos Chem Phys, 11(5), 2245–2279, 2011.

Sorem, R. K.: Volcanic ash clusters: Tephra rafts and scavengers, J. Volcanol. Geotherm. Res., 13(1), 63–71, doi:10.1016/0377-0273(82)90019-1, 1982.

Sparks, R. J. S., Burski, M. I., Carey, S. N., Gilbert, J. S., Glaze, L. S., Siquerdsson, H. and Woods, A. W.: Volcanic Plumes, John Wiley and Sons, Sussex, England., 1997.

Stevenson, J. A., Loughlin, S., Rae, C., Thordarson, T., Milodowski, A. E., Gilbert, J. S., Harangi, S., Lukács, R., Højgaard, B., Árting, U., Pyne-O'Donnell, S., MacLeod, A., Whitney, B. and Cassidy, M.: Distal deposition of tephra from the Eyjafjallajökull 2010 summit eruption, J. Geophys. Res. Solid Earth, 117(B9), doi:10.1029/2011JB008904, 2012.

Stockwell, W. R., Middleton, P., Chang, J. S. and Tang, X.: The second generation regional acid deposition model chemical mechanism for regional air quality modeling, J. Geophys. Res., 95(D10), 16343–16,367, doi:10.1029/JD095iD10p16343, 1990.

Stohl, A., Prata, A. J., Eckhardt, S., Clarisse, L., Durant, A., Henne, S., Kristiansen, N. I., Minikin, A., Schumann, U., Seibert, P., Stebel, K., Thomas, H. E., Thorsteinsson, T., Tørseth, K. and Weinzierl, B.: Determination of time-and height-resolved volcanic ash emissions and their use for quantitative ash dispersion modeling: the 2010 Eyjafjallajökull eruption, Atmos Chem Phys, 11(9), 4333–4351, doi:10.5194/acp-11-4333-2011, 2011.

Stuefer, M., Freitas, S. R., Grell, G., Webley, P., Peckham, S., McKeen, S. A. and Egan, S. D.: Inclusion of ash and SO 2 emissions from volcanic eruptions in WRF-Chem: development and some applications, Geosci. Model Dev., 6(2), 457–468, doi:doi.org/10.5194/gmd-6-457-2013, 2013.

Taddeucci, J., Scarlato, P., Montanaro, C., Cimarelli, C., Bello, E. D., Freda, C., Andronico, D., Gudmundsson, M. T. and Dingwell, D. B.: Aggregation-dominated ash settling from the Eyjafjallajökull volcanic cloud illuminated by field and laboratory high-speed imaging, Geology, 39(9), 891–894, doi:10.1130/G32016.1, 2011.

Textor, C., Graf, H. F., Herzog, M., Oberhuber, J. M., Rose, W. I. and Ernst, G. G. J.: Volcanic particle aggregation in explosive eruption columns. Part I: Parameterization of the microphysics of hydrometeors and ash, J. Volcanol. Geotherm. Res., 150(4), 359–377, doi:10.1016/j.jvolgeores.2005.09.007, 2006.

Thomas, H. E. and Prata, A. J.: Sulphur dioxide as a volcanic ash proxy during the April–May 2010 eruption of Eyjafjallajökull volcano, Iceland, Atmos Chem Phys, 11(14), 6871–6880, 2011.

Thordarson, T. and Self, S.: Atmospheric and environmental effects of the 1783–1784 Laki eruption: A review and reassessment, J. Geophys. Res. Atmospheres, 108(D1), AAC 7-1-AAC 7-29, doi:10.1029/2001JD002042, 2003.

Van Eaton, A. R., Muirhead, J. D., Wilson, C. J. and Cimarelli, C.: Growth of volcanic ash aggregates in the presence of liquid water and ice: an experimental approach, Bull. Volcanol., 74(9), 1963–1984, 2012.

Van Eaton, A. R., Mastin, L. G., Herzog, M., Schwaiger, H. F., Schneider, D. J., Wallace, K. L. and Clarke, A. B.: Hail formation triggers rapid ash aggregation in volcanic plumes, Nat. Commun., 6, 7860, doi:10.1038/ncomms8860, 2015.

Von Smoluchowski, M.: Investigation of a Mathematical Theory on the Coagulation of Colloidal Suspensions, Z Phys. ChemGer, 92, 155, 1917.

Waitt, R. B., Hansen, V. L., Sarna-Wojcicki, A. M. and Wood, S. H.: Proximal air-fall deposits of eruptions (of Mount St. Helens) between May 24 and August 7, 1980 - stratigraphy and field sedimentology., US Geol. Surv. Prof. Pap., 1250, 617–628, 1981.

Wallace, K. L., Schaefer, J. R. and Coombs, M. L.: Character, mass, distribution, and origin of tephra-fall deposits from the 2009 eruption of Redoubt Volcano, Alaska—Highlighting the significance of particle aggregation, J. Volcanol. Geotherm. Res., 259, 145–169, doi:10.1016/j.jvolgeores.2012.09.015, 2013.

Webley, P. W., Steensen, T., Stuefer, M., Grell, G., Freitas, S., Pavolonis, M.: Analysing the Eyjafjallajökull 2010 eruption using satellite remote sensing, lidar and WRF-Chem dispersion and tracking model, J. Geophys. Res. Atmospheres, 117(D20), doi:10.1029/2011JD016817, 2012.

Young, C. L., Sokolik, I. N. and Dufek, J.: Regional radiative impact of volcanic aerosol from the 2009 eruption of Mt. Redoubt, Atmospheric Chem. Phys., 12(8), 3699–3715, doi:10.5194/acp-12-3699-2012, 2012.

Figures

Commented [SDE14]: Figure captions have been updated to meet Copernicus guidelines such that panel labels are lowercase.

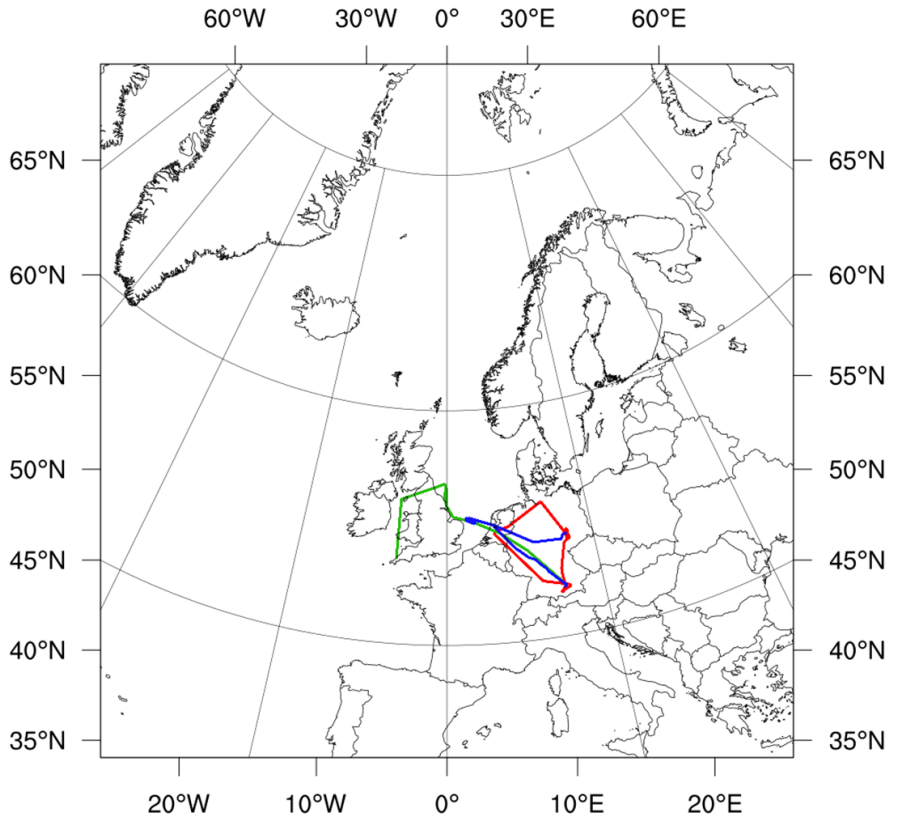

Figure 1: WRF-Chem model domain used for simulations in Lambert Conformal projection with true latitude and longitude and center at 0°E/W, 50°N. Location of Eyjafjallajökull (63.62°N, 19.61°W) marked with red dot. DLR Falcon flight paths for flights on April 19 (red), May 16(green) and May 17(blue) shown with colored lines.

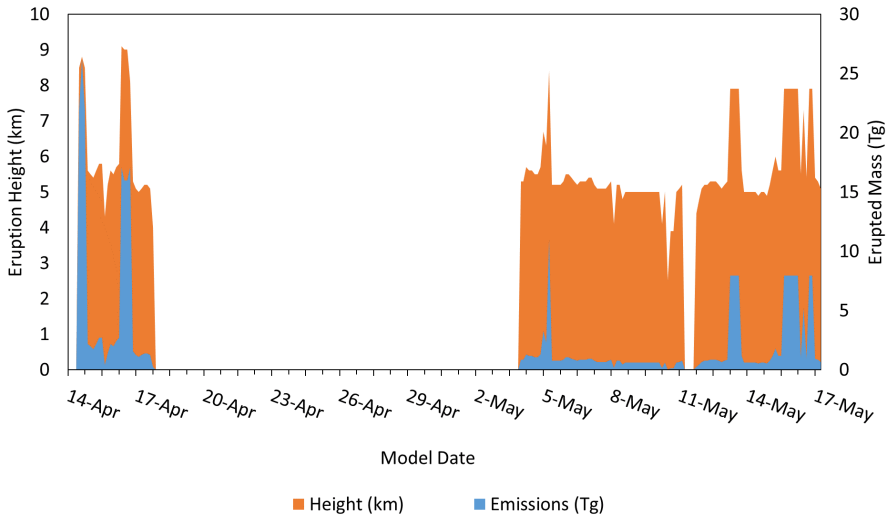

665

Figure 2: Three hourly plume heights (KM) ASL (orange, km) and emitted mass (blue, Tg) used in the WRF-Chem modeling simulations (volc_d01.asc name list) for the eruption period April 12 until May 18, 2010. Values adapted from Hirtl et al., (2019) with dates as DD/MMM.

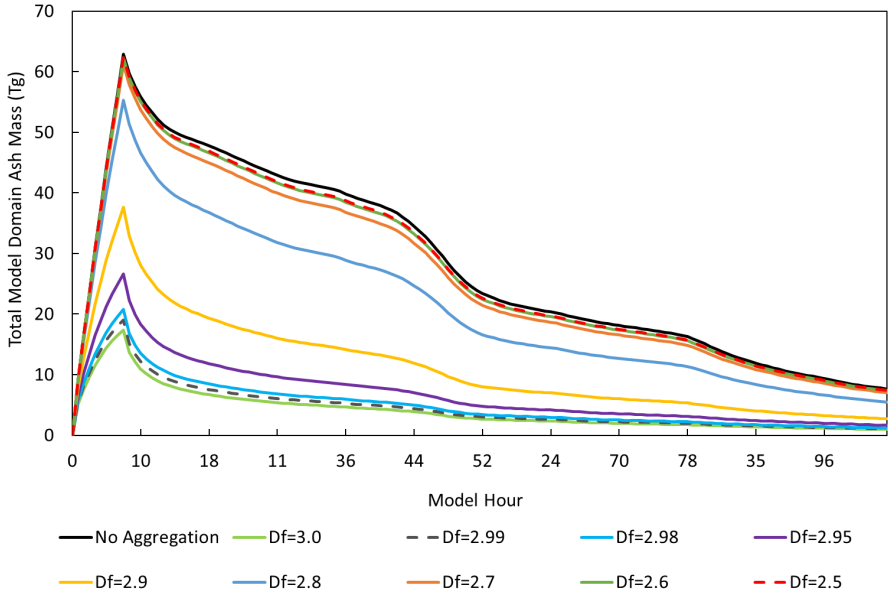

670

Figure 3: Change in total domain ash mass, Tg, for a hypothetical eruption on May 5th, beginning 00:00Z and ending 09:00Z, for a range of fractal dimensions, D_f = {3.0, 2.99, 2.98, 2.95, 2.9, 2.8, 2.7, 2.6, 2.5}. Constant eruption rate = 4 x 10^6 kg s^{-1}.

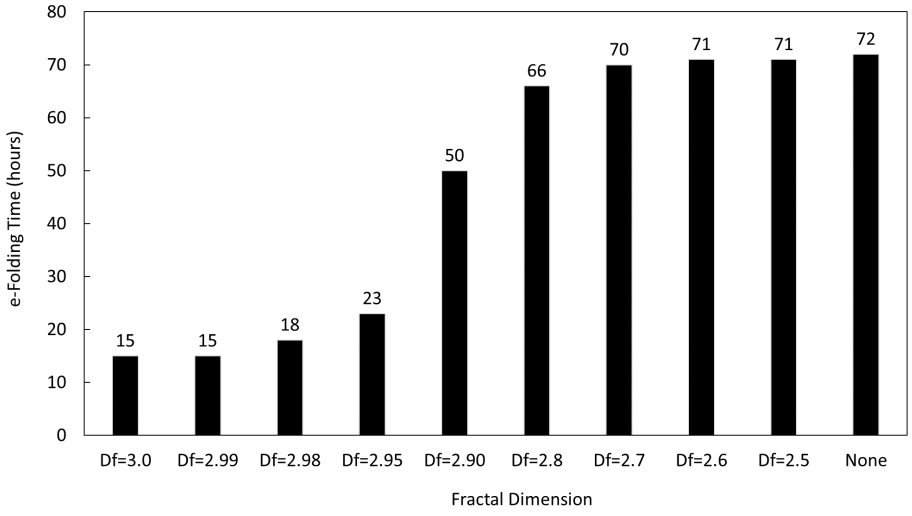

675

Figure 4: Volcanic ash e-folding time in hours for a hypothetical eruption on May 5th, beginning 00:00Z and ending 09:00Z, for a range of fractal dimensions, D_f = {3.0, 2.99, 2.98, 2.95, 2.9, 2.8, 2.7, 2.6, 2.5}. Constant eruption rate = 4 x 10^6 kg s^{-1}.

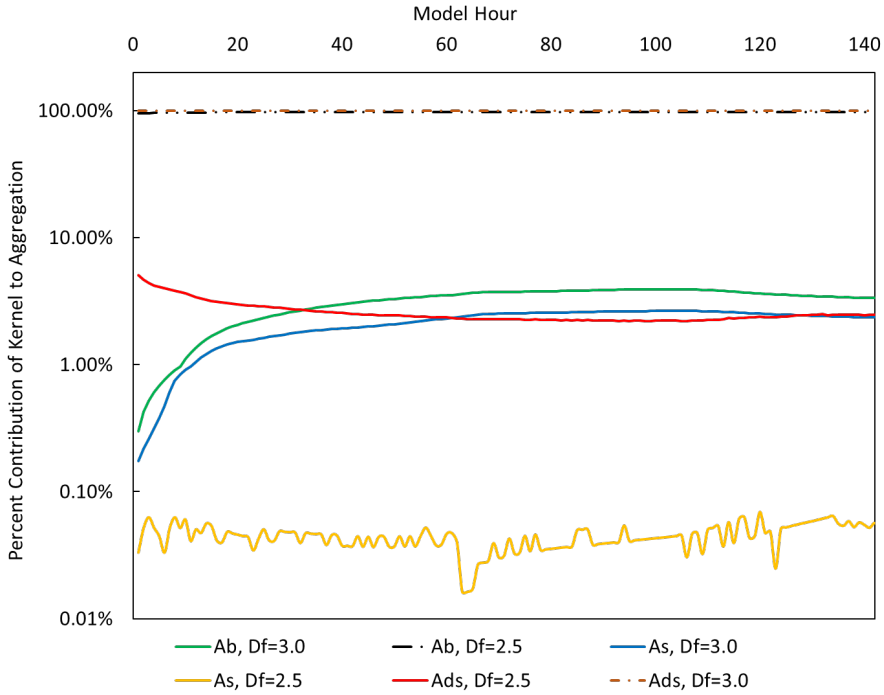

680 **Figure 5: Percentage of aggregation rate for each collision kernel (A_B = Brownian, A_S = Shear, A_{DS} = Differential Sedimentation) when considering a hypothetical eruption on May 5th, beginning 00:00Z and ending 09:00Z, for two fractal dimensions, D_f = {3.0, 2.5}. Constant eruption rate = 4 x 10^6 kg s^{-1}.**

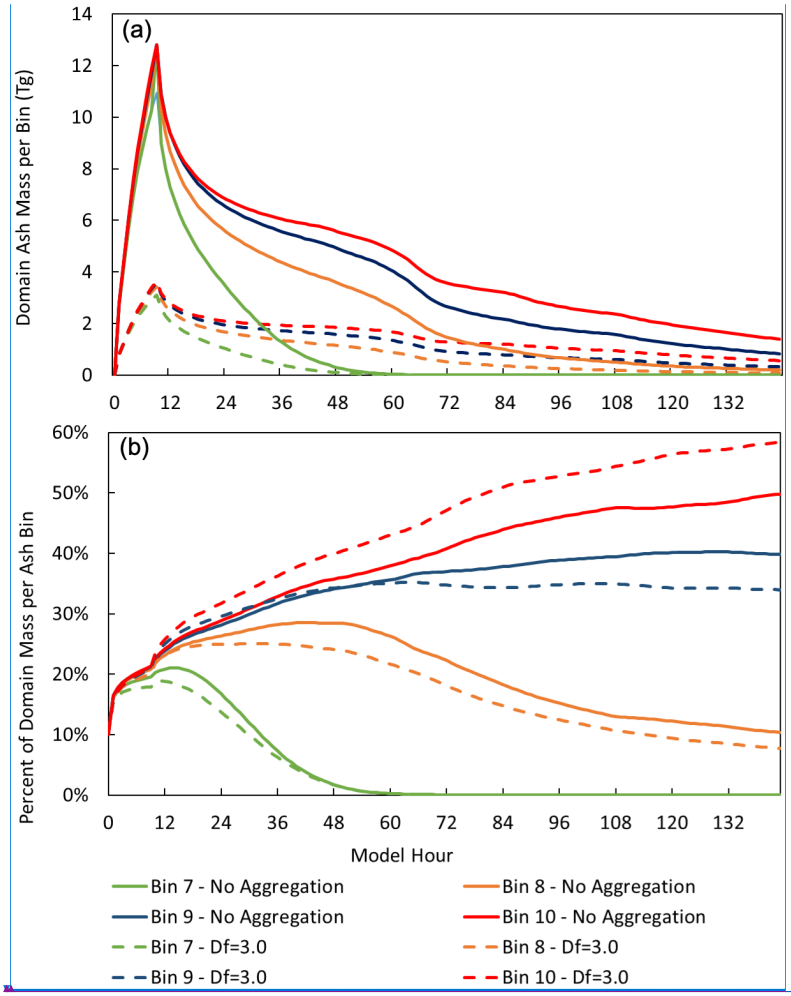

685 **Figure 6:Total domain mass (a) and particle size distribution (b) of volcanic ash bins 7 to 10 when considering a hypothetical eruption on May 5th, beginning 00:00Z and ending 09:00Z, and a fractal dimensions, D_f = 3.0. Constant eruption rate = 4 x 10^6 kg s^{-1}.**

Commented [SDE15]: We labelled each panel (a and b) and also removed the grey line that existed between the panels to help clarify that the legend applies to both subplots

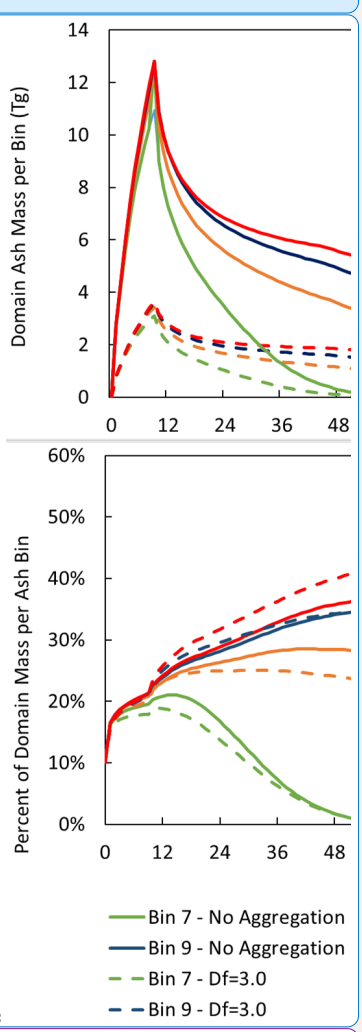

Deleted:

Formatted ... [1]

Deleted: A... and particle size distribution (bB ... [2]

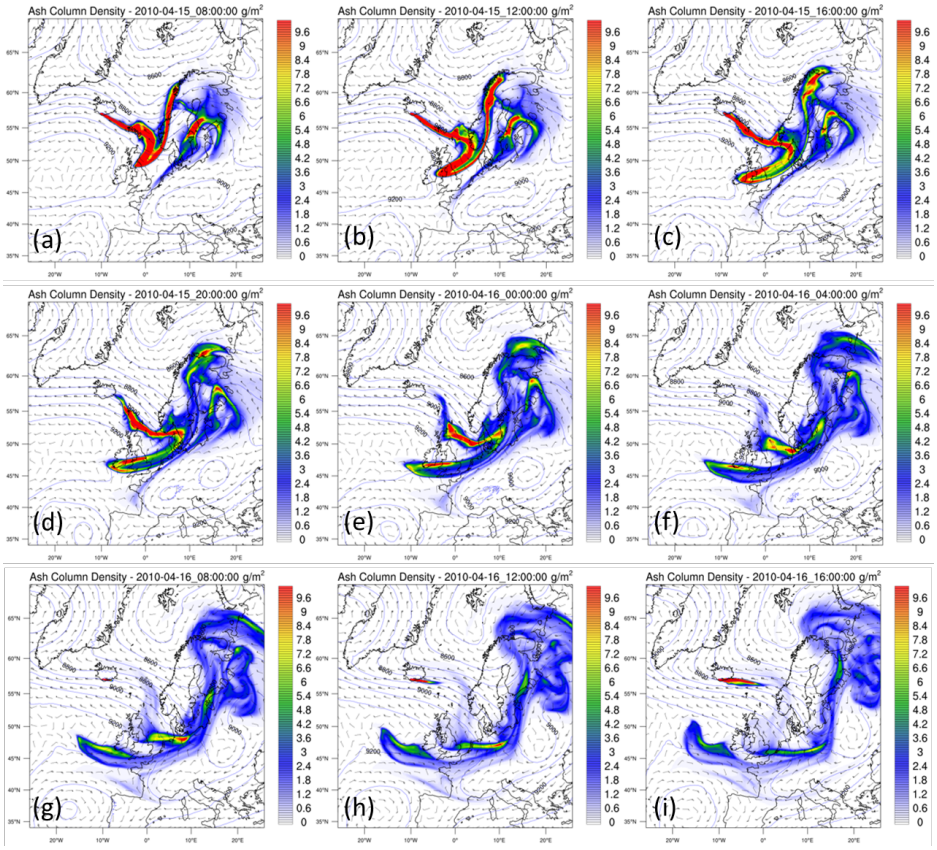

Figure 7: WRF-Chem generated volcanic ash column densities for the Eyjafjallajökull eruption in April 2010 at four hour intervals, (a) = April 15 at 08 UTC, (b) = April 15 at 12 UTC, (c) = April 15 at 16 UTC, (d) = April 15 at 20 UTC, (e) = April 16 at 00 UTC, (f) = April 16 at 04 UTC, (g) = April 16 at 08 UTC, (h) = April 16 at 12 UTC, and (i) = April 16 at 16 UTC.

Deleted: A
Deleted: B
Deleted: C
Deleted: D
Deleted: E
Deleted: F
Deleted: G
Deleted: H
Deleted: I
Deleted: Note each time output is at 00 hr.

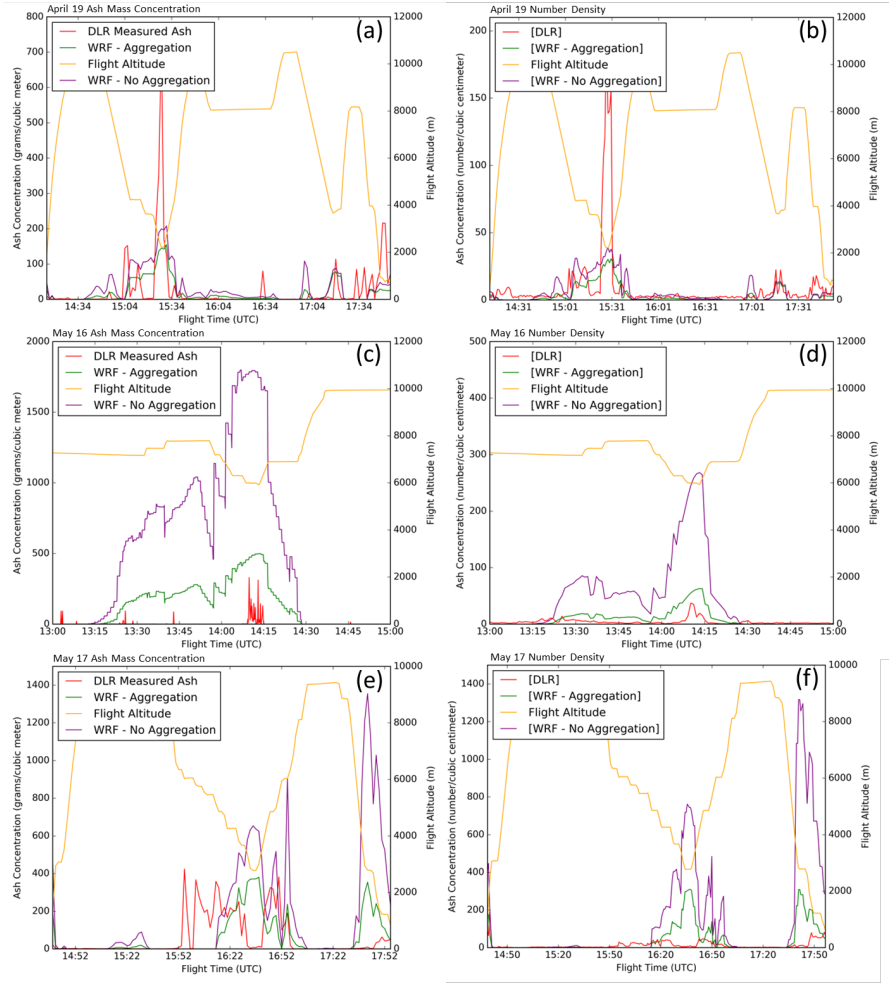

Figure 8: Comparisons of WRF-Chem model output to in situ mass concentrations (left panels) and particle numbers (right panels) observed by DLR during April 19 (a and b), May 15 (c and d) and May 17 (e and f), 2010 flights.

Deleted: A

Deleted: B

Deleted: C

Deleted: D

Deleted: E

Deleted: F

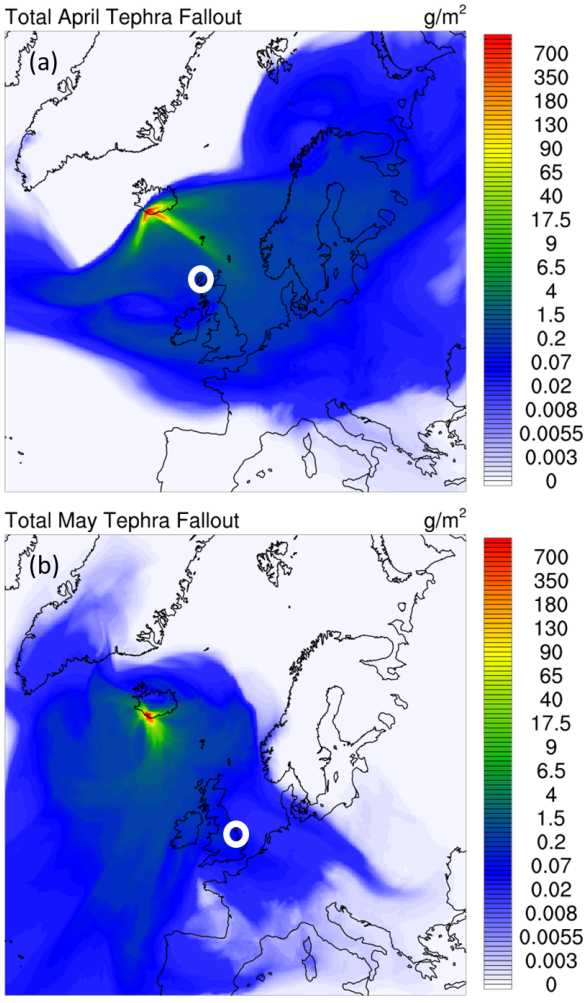

Figure 9 Mass of tephra fallout deposited on model surface, lowest model level in WRF-Chem, for April (A,) and May (B) 2010 model simulations. White circle in (a) marks the Outer Hebrides and white circle in (b) marks Lincolnshire and Leicestershire, UK, corresponding to sample areas in Stevenson et al., (2012). Maximum domain fallout is 52 Mg m^{-2}.

Deleted: A

Deleted: B

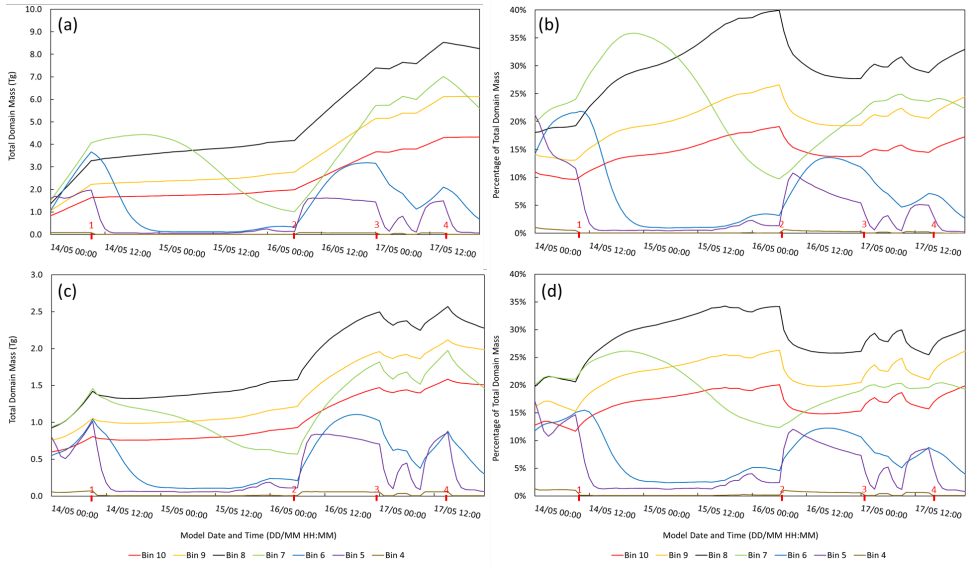

Figure 10: Total domain ash mass (a, c) and percent contribution to domain mass (b, d) for the modeled period between 14 and 18 May, 2010 without (a, b – upper panels) and with (c, d – lower panels) aggregation code enabled. Red numbers on date/time axis denote major (> 10%) changes in the eruption rate: 1) 14/09Z - Decrease from 7.949 to 1.775 Tg/3 hours, 2) 16/06Z - Increase from 1.175 to 7.949 Tg/3 hours, 3) 17/00Z - Decrease from 7.949 to 1.056 Tg/3hours, 4) 17/15Z - Decrease from 7.949 to 0.966 Tg/3hours. Note there are variable increases and decreases in the eruption rate between times 3 and 4.

Deleted: A
Deleted: C
Deleted: B
Deleted: D
Deleted: A
Deleted: B
Deleted: C
Deleted: D

Tables

Table 1 – *Derived coagulation kernel equations used in the calculation of* ΔN.

Kernel	Equation (#)	Variables and Units
Brownian Motion	$A_B = \frac{4kT}{3\mu}$ (3)	k_b– Boltzmann Constant - m^2 kg s^{-1} K^{-1} T – Temperature – K μ – Dynamic Viscocity - kg m^{-1} s^{-1} d – Diameter - m
Fluid Shear	$A_S = -\frac{2}{3}\xi^3 \Gamma_S$ (4)	Γ_s - Fluid Shear – s^{-1} d – Diameter – m ξ – Fractal Dimension Factor
Differential Sedimentation	$A_{DS} = \frac{\pi(\rho_p - \rho)g}{48\mu}\xi^4$ (5)	d – Diameter – m ξ – Fractal Dimension Factor ρ – Density of Air ρ_p – Density of primary particle V_d - Fall Velocity – m s^{-2}

Table 2 – *Ash aggregation coefficients based on liquid water content, w/w, as described in Van Eaton et al., (2012). The weight percent of water (w/w) is calculated as mass of water divided by mass of the atmosphere.*

Liquid Water Content (w/w)	Corresponding S value
0% (ice)	0.020
0-10%	0.008
10-15%	0.004
15-25%	0.002

745

Table 3 – *Distribution of volcanic ash in model domain among 10 size bins corresponding to the S2 size distribution as given in Mastin et al. (2009). The percentages of mass per bin are specified in the volc_d01.asc name list and may be given any value between 0 and 100.*

Bin	Diameter	Percent Mass
1	1-2 mm	22.0
2	0.5-1 mm	5.0
3	0.25-0.5 mm	4.0
4	125-250 μm	5.0
5	62.5-125 μm	24.5
6	31.25-62.5 μm	12.0
7	15.625-31.25 μm	11.0
8	7.8125-15.625 μm	8.0
9	3.9065-7.8125 μm	5.0
10	<3.9065 μm	3.5

Deleted: .

Table 4 – *Details of the model sensitivity studies discussed, including parameters varied and the analysis methodology.*

Sensitivity Study Analysis Variable	Analysis Method
Total Domain Mass	Integrate ash mass over entire domain, calculate change in mass over time.
Fractal Dimension, D_f	Vary D_f by setting to 2.5, 2.6, 2.7, 2.8, 2.9, 2.95, 2.98, 2.99, 3.0. Analyze change in domain mass using each value.
Collision Kernel	Run aggregation code with each collision kernel, A_B, A_S and A_{DS} enabled independently. Analyze change in domain mass for each.
Water Vapor Emissions	Ran model with and without enabling water vapor emissions. Analyze change in domain mass for each.

Formatted: Font: Italic

Code Availability

This work modified the Weather Research Forecasting with Chemistry (WRF-Chem) base code. This included the creation and modification of text and Fortran files that replace and augment existing WRF-Chem code. These files may be accessed using the DOI reference provided upon publication of the code at doi:10.5281/zenodo.3540446. Code modifications along with descriptions are also directly available from the author upon request.

List of Changes

Line 30: Fixed grammar in reply to reviewer 2.

Line 32: Added a list of plume characteristics as requested by reviewer 2.

Line 38: Changed word “edge” to corner as suggested by reviewer 2.

Line 96: Reviewers were asking how or if WRF can be used operationally for aircraft hazard mitigation. We state here that it may be used to augment current VATD models (rather than used alone).

Line 145: Added reference to Table 1 as requested by Reviewer 2.

Line 167: Removed bold face font on math terms.

Line 169, 186: Updated equation numbers.

Line 187: Added reference to Table 3 as requested by Reviewer 2.

Line 213: Added word “radar” as requested by Reviewer 2.

Line 223: Added clarification of the 10km^2 resolution as requested by Reviewer 1 and 2 and specified by editor.

Line 233: Added clarification of the choice of 48 hour meteorology field updates, as requested by Reviewers 1 and 2. (We were very limited in our access to computational resources).

Line 253: Added new Table 4 as requested by Reviewer 2.

Line 259: Clarified why 24 hour updates were used as requested by both reviewers.

Line 294: Comment on Reviewer 2 questions as to whether or not a fractal dimension of 3.0 is realistic. We argue here that it is.

Line 309: Comment on Reviewer 1 requesting a study on plume travel distance. We argue here that the lifetime analysis does this.

Line 354: Updated figure references as requested by Reviewer 2.

Line 355: Updated “cast” to “show” as requested by Reviewer 2.

Line 368: Added discussion of the peak concentration observed by DLR that was not resovled by WRF as requested by both reviewers.

Line 409: Updated figure labels as requested by Reviewer 2.

Line 433: Both reviewers asked if wet deposition is included in WRF. We had a line in the original text that made it sound like it is not by saying gravitational settling is the only sink – we clarified this here to add that the settling routine does take into account water vapor, so removal is affected by this term.

Line 450: Reviewers questioned what the impact of the different collision kernels on aggregation are. We state this here by noting that vertical motion, correlated to the differential sedimentation kernel, is the driving force behind aggregation.

Line 484: Additional text was added to further clarify that this study was on the distal ash transport, which was questioned by Reviewers 1 and 2 (proximal resolution vs distal resolution).

Line 490: Listed examples of global models for clarification as requested by Reviewer 2.

Figures – Updated all subpanel reverences to match case as requested by Reviewer 2.

Figure 6 – Corrected line that separated both panels to clarify that the legend applies to both as requested by Reviewer 2.

Table 4 – Added new table with summary of sensitivity studies as requested by Reviewer 2.

Replies to Referee One:

Comment 1: “Is the 10x10 km grid size adequate to discribe the near-source aggregates (<15km distance from the volcano)? Could you consider a nested higher resolution grid over Iceland to address these processes? This may not be important for the long range transport since anyhow the bigger particles will be removed from the model but it could provide more insight on the processes and probably improved deposition fluxes near the erruption.”

This study built off work by Costa et al. (2010) and Folch et al. (2010, 2015) who used the simplified version of the Smoluchowski equation in this work to study near vent deposition. As such, our efforts focused on the study of ash aggregation processes’ effects on distal volcanic ash transport, so attention was paid to the distal plume. The large spatial extent necessary for studying the distal plume required a lower resolution to allow for feasible computational times.

WRF-Chem is capable of much higher resolution model studies and these parameters could be used to study near vent aggregation phenomena, like was done in Costa et al. (2010) and Folch et al. (2010). Furthermore, this study could benefit from a nested domain over the vent, however this was computationally not feasible with the compute time available to our group.

The conclusions section of the paper has been updated to include:

“As stated, the majority of volcanic ash aggregation occurs proximally, especially when high water vapor concentrations are present in the eruptive column. Future studies of volcanic ash near the vent should consider including a nested, high resolution domain over the source to allow for the study of proximal ash fall. We will add a discussion of this to the conclusions portion of the paper in order to highlight the capability of WRF-Chem to include nested, high resolution domains, and add that the equations used also apply to near vent, proximal aggregation.”

Comment 2: “Please check that the references are provided in chronological order throughout the text.”

All references have been updated chronologically.

Comment 3: “In line 92 " As an example, FALL3D is typically initialized with a WRF model run that is executed prior to the dispersion model. Modeling particle dispersion with WRF-Chem is, therefore, as computationally feasible as running these models since in many cases, a mesoscale, gridded model must be run for their initialization". Indeed, but you can run multiple faster Lagrangian dispersion simulations with different configurations using a single meteorological output (e.g. WRF) which may be important for determining aviation hazard under different emission scenarios.”

We agree with your comment and will revise the text. Lagrangian dispersion models clearly have their place in aircraft hazard mitigation, especially since they can provide a number of different solutions based on perturbed initial conditions with relatively little computational requirement. The wording of the background has changed to include:

"WRF-Chem may augment Lagrangian dispersion models by providing output that is constrained by a number of physical processes, to include aggregation, that are typically not included in dispersion models. Additionally, WRF-Chem may benefit research modeling, allowing researchers to study the effects of numerous microphysical processes on volcanic ash, including aggregation, as well as environmental feedback such as those discussed by Hirtl et al. (2015)."

Comment 4: "One peak concentration was observed at 15:30 UTC on April 19, which was not re- solved by WRF-Chem (Fig. 8b). Typical of any Eulerian air quality model, WRF-Chem tends to diffuse ash concentrations, an effect that is also dependent on the model res- olution." I suggest that you should elaborate more on this mismatch between model and observed ash concenntrations. Such high peaks are the primary threat for aviation and moreover these are observed at about 2km elevation which may imply approach or takeoff heights thus increasing the potential danger. This may not be due to Eulerian diffusion otherwise one would expect a more uniform reduction of the concentration fields. Could you please check the concentration at the surounding gridpoints to check if possibly such concentrations exist and are misplaced by the model ?"

We did an analysis of the surrounding grid cells. Laterally there was agreement in the model output with decreased ash seen in the i and j directions. Vertically, however, there was an increase in ash seen aloft, however it was not as extensive as the DLR observed peak. We believe this is Eulerian diffusion since the areas under the curve between the times at this peak agree between the model and observations. The text has been updated to include:

"An analysis of the surrounding grid cells in the vertical and horizontal did not contain this peak, however the next vertical grid cell in the positive k contained higher ash concentrations. This analysis, along with analysis of the integrated volcanic ash over the time span of the peak, lead to the conclusion that this the lack of peak concentration in the model is a result of model diffusion."

Comment 5: "Without aggregation, the only sinks for volcanic ash are via settling or via the plume traveling out of the model domain." . Don't you condider also the wet removal from incloud and below cloud processes?"

The volcanic ash settling routing included in WRF-Chem does remove ash faster in the presence of water vapor. It does this by increasing the effective size of the particles, and therefore the fallout rate of ash, with increasing relative humidity. There

is no coupling to rain effects, however, such that rain interactions with volcanic ash are not included. Only the relative humidity fields are taken into account. The text was updated as follows:

"Without aggregation, the only sinks for volcanic ash are via settling, which is dependent on gravity and water vapor concentration, or via the plume traveling out of the model domain."

Comment 6: "I would suggest to extend the sensitivity analysis including not only the total domain mass but also the maximum traveling range from source for the various bins."

Because e-folding time is correlated with distance, a distance sensitivity study would be a recast of this data. The paper may benefit from another figure that details this in terms of distance for each bin, however. We will consider doing so for each bin and if generated will be referenced in the discussion alongside the current e-folding time sensitivity study analysis.

Replies to Referee Two:

Each referee comment is replied to separately:

Reply to general comments:

General Comment1: “Should aggregation uncertainty be considered in an emergency response situation?”

As mentioned in the paper, aggregation can reduce the total erupted mass substantially, which will reduce the total atmospheric loading of both proximal and distal ash. For example, we reference Van Eaton et al. (2015), who detailed rapid aggregation of proximal ash at the onset of the eruption of Mount Redoubt. This reduces the total amount of both proximal and distal volcanic ash. Aircraft hazard mitigation involves placing limits on the concentration of volcanic ash that commercial aircraft may encounter. Including volcanic ash aggregation into WRF-Chem, as well as other dispersion models, allows it to capture a more realistic change in the concentration of ash with time, and therefore more realistic volcanic ash concentrations. Therefore, if an Eulerian model is used in an emergency response, it would benefit from the inclusion of this important microphysical process. The text has been updated to reflect this by including the following discussion to the background:

“Volcanic ash aircraft hazard mitigation typically focuses on limiting commercial aircraft to ash concentration thresholds (Casadevall, 1994). WRF-Chem solves the advection equations such that ash concentration is tracked over time. This ability to track volcanic ash mass, rather than particle number, augments current VATD models and offers another tool to constrain atmospheric ash loading.”

General Comment 2: “Aggregation will only reduce the distal ash concentrations so maybe computational effort should be put into performing ensemble simulations that vary eruption plume height or the meteorological situation.”

This is a valid approach for modeling volcanic ash dispersion which is already in use. Volcanic ash plume models such as the aforementioned FPLUME-1.0 detailed by Folch et al. (2015), for example, run a computationally inexpensive set of calculations that results in parameters which can be input into volcanic ash dispersion models. FPLUME, in addition, includes parameterizations for volcanic ash aggregation, allowing the forecasting of the resulting particle size distribution in long range deterministic and ensemble models.

While this approach is valid and useful for a number of applications, the integration of volcanic ash aggregation into WRF-Chem has distinct benefits. First, WRF-Chem can be used to study a number of physical processes involved with the suspension and transport of volcanic ash in the atmosphere, such as the radiation feedbacks studied by Hirtl et al. (2019) that we mention

in the introduction. Including an aggregation option in WRF-Chem allows researchers to include this important microphysical process into the model's treatment of parameterized volcanic ash particle size distributions. Second, volcanic plume models initialize a particle size distribution based on a number of physical processes, to include aggregation. These distributions are then carried forward in the calculations as the proximal plume becomes distal. At this time, the calculations that change the particle size distribution in the distal plume are only based on advection and gravitational settling equations. Aggregation equations allow for another important sink to be considered in the modeling of distal plume ash concentrations.

General Comment 3: "Can WRF-Chem be run in real-time emergency response situation?"

WRF-Chem has not yet been used in an emergency response situation, but it is feasible to consider it for such a purpose. With continued increases in computational power, solving for fully coupled, Eulerian solutions has become increasingly cheap. In our studies, a 4 day simulation with 48 hour spin up time using the model parameters detailed in the paper required less than 20 minutes to complete using 512 processing cores. This could augment current Lagrangian particle dispersion models which are able to provide instant results by providing volcanic ash concentrations which take into account not only gravitational settling and wet deposition, but also aggregation processes.

General Comment 4: "What over head is added by including the representation of aggregation?"

The added overhead from the aggregation code is minimal. Because the integration has been reduced to a set of simple algebraic computations, the resulting increase in model time is less than 5%. These effects scale with domain size and a parametric study could be conducted to show the overall increase in overhead with number of cores and domain size.

Text Comment 1: "L29: Missing "and" between tools, the study of ash physics"

These lines have been updated appropriately.

Text Comment 2: "L30: Could state what the characteristics of the plume are required for modelling."

These are enumerated later in the text during the model setup, however we updated line 30 to clarify further as follows:

"Numerical models have been developed to better describe the initial plume characteristics of eruptions, such as plume height, shape, mass loading and particle size distribution, which are all necessary parameters for ash forecasting. "

Text Comment 3: "L37: Unsure what you mean by plume corner here"

This terminology has been changed to “edge”. The term “corner” stemmed from the use of the model grid cell “corner” that acted as the start and end of the distance calculation.

Text Comment 4: “L95-102: The text here seems a bit clumsy with section numbers and headings men- tioned Would it be possible to include the equations and associated parameters in Table 1 in the main body of text? It would make it easier to follow.”

The equations in Table 1 are mostly referenced in the text to follow, so we are hesitant to move it farther up, but we will discuss with our editor how to best follow up on this comment.

Text Comment 5 and 6: “L163: This should be equation 6; L180: This should be equation 7”

These equation references have been corrected.

Text Comment 7: “L181: Refer to Table 3 so the reader knows the particle sizes that the bins refer to.”

A reference to Table 3 has be added for clarity.

Text Comment 8: “L205: “radar” missing”

This word radar has been added after Doppler.

Text Comment 10: “L216: You refer to 10km2 as high resolution. This maybe true when considering long range dispersion but is it high enough for modelling aggregation near the eruption plume?”

Our study was primarily focused on the dispersion of distal volcanic ash. For a study of near vent volcanic ash fallout, one could use a nested domain with a much higher, for example less than 1 square kilometer, resolution. We now address this in the paper by including the following text:

“As stated, the majority of volcanic ash aggregation occurs proximally, especially when high water vapor concentrations are present in the eruptive column. Future studies of volcanic ash near the vent should consider including a nested, high resolution domain over the source to allow for the study of proximal ash fall. We will add a discussion of this to the conclusions portion

of the paper in order to highlight the capability of WRF-Chem to include nested, high resolution domains, and add that the equations used also apply to near vent, proximal aggregation."

Text Comment 11: "L223: Are 48 hourly meteorological initialisations frequent sufficient?"

These could be more frequent. The choice of 48 hour re-initializations was chosen to offset the very large lag time that was required by the computation cluster in use. Every time WRF was re-initialized the model first had to checkout processors from the cluster. The cluster we used sometimes would queue these jobs for days before launching. Additionally, the 48 hour re-initialization was used by a study of volcanic ash using WRF-Chem by Hirtl et al. (2019) who observed good results with this interval.

Text Comment 12: "L244: Why change from 48 hours to 24 hours?"

The sensitivity study covered only 6 days which allowed for 24 hour re-initializations. We briefly discuss that this choice is to make the sensitivity study "higher fidelity".

Text Comment 13: "L245: A table outlining the different sensitivity studies would aid the reader here."

The following table has been added to the text to make this more clear.

Sensitivity Study Analysis Variable	Analysis Method
Total Domain Mass	Integrate ash mass over entire domain, calculate change in mass over time.
Fractal Dimension, D_f	Vary D_f by setting to 2.5, 2.6, 2.7, 2.8, 2.9, 2.95, 2.98, 2.99, 3.0. Analyze change in domain mass using each value.
Collision Kernel	Run aggregation code with each collision kernel, A_B, A_S and A_{DS} enabled independently. Analyze change in domain mass for each.

Water Vapor Emissions	Ran model with and without enabling water vapor emissions. Analyze change in domain mass for each.

Text Comment 14: "L275: How representative is a Df=3.0 of the real world? Does Df vary from volcano to volcano?"

This is discussed briefly in the text and will be elaborated upon more. For example, we mention that Folch et al. (2010) detail the correlation between Df and the aggregation rate using an aggregation enabled version of Fall3D. We will expand the discussion with their finding that Df=2.99 was realistic in the cases their study covered. Additionally, the sensitivity study shows little difference in the aggregation rate between Df=3.0 and Df=2.99.

Text Comment 15: "L285: Why is the difference between 2.8 and 3.0 highlighted here. Is this unexpected?"

We are highlighting the change in lifetime seen with varying fractal dimension. Only minimal changes in atmospheric residence time are seen with Df<2.8. The lifetime decreases substantially for Df=2.8 and greater. This is also noted in other studies mentioned in the paper where Df was varied across a range.

Text Comment 16: "L294: Is this jump that is highlighted unexpected?"

It is expected, based on the parametric studies included in Costa et al. (2010).

Text Comment 17: "L306: What are the implications for the different processes being dominant?"

This observation was also noted in Costa et al. (2010) in their parametric study. The main implication is that the contribution from the shear kernel is minimal, and therefore could be disregarded in the calculations.

Text Comment 18: "L317: The small effect of coupling the aggregation to water emissions seems impor- tant. Should this be highlighted more or is it very dependent on the volcano?"

This study focused primarily on the effects of aggregation in the distal plume. Despite the large amount of water vapor emitted from Eyjafjallajökull during its eruptive phases, the overall contribution to atmospheric water vapor as noted from total precipitable water observations during that time were minimal. A study of the effect of water vapor on proximal ash during

the first minutes and hours of the eruption would likely show a greater effect, but the distal plume ends up dry due to the entrainment of dry air by the proximal plume.

Text Comment 19: “L334: 3.9 should be 8.”

This has been corrected.

Text Comment 20: “L334/335: Unsure of the use of “cast”, “show” would be clearer.”

The wording has been changed as suggested.

Text Comment 21: “L345: How much computational expense? Do you have plans to do this?”

Decreasing the grid cell size increases the computational time slightly more than linearly due to the added communication between compute nodes. This is a known drawback to Eulerian models and we do not plan to resolve these with more higher resolution runs.

Text Comment 22: “L346: What does 9C refer to?”

This should read Figure 8c. This has been corrected.

Text Comment 23: “L350: Why do you think that there is such a discrepancy between the observations and WRF-CHEM during this time?”

We put significant effort into ensuring that this was not an analysis error. The vertical resolution of the model domain is much lower than the horizontal resolution with the most significant spread near the 500mb level. The larger uncertainty in the vertical resulted in differences in the concentration during the transect that were larger than the translational transects, in general. Increasing the vertical resolution of the model increases the computational cost exponentially, as opposed to the near linear increase experienced from increasing horizontal resolution. The text has been updated to include the following discussion:

“An analysis of the surrounding grid cells in the vertical and horizontal did not contain this peak, however the next vertical grid cell in the positive k contained higher ash concentrations. This analysis, along with analysis of the integrated volcanic ash over the time span of the peak, lead to the conclusion that this the lack of peak concentration in the model is a result of model diffusion.”

Text Comment 24: “L377: 11(d) should be 10(d):

This has been corrected

Text Comment 25: “L400: Is wet deposition represented in WRF-CHEM? This can have a large impact on the long-range plume development.”

The volcanic ash settling routine in WRF-Chem does consider wet deposition by increasing the effective radius of the particles, and thus their fall rate, with increasing relative humidity. The following discussion has been added to make this more clear:

“Without aggregation, the only sinks for volcanic ash are via settling, which is dependent on gravity and water vapor concentration, or via the plume traveling out of the model domain.”

Text Comment 26: “L450: Unsure what is meant by global models here”

This is in reference to global spectral models, such as the Global Forecast System run by the National Centers for Environmental Prediction and Integrated Forecast System run by the European Center for Medium-Range Weather Forecasts.

Figure Comment 1: “There seems to be a mismatch between using lower case labels on plots and capital letters in the captions. Please make these consistent.”

These figure labels have been updated as suggested.

Figure Comment 2: “Figure 5: Think about colouring lines to make it easier for the reader to compare lines with same Df.”

We updated the color schemes with a few different options and will discuss them with the editor to find the best for the final version.

Figure Comment 3: “Figure 6: The subfigure labels are missing. There seems to be a grey bar between the panels. Reorder the legend to make it easier for the reader (e.g. No aggregation all in same column)”

These figures have been corrected to include all labels and are separated by column.

Figure Comment 4: “Figure 7: Rainbow colour scales are not suitable for people who have colour blindness. Please considering using a different colour scale. Unsure what “Note each time output is at 00hr” means.”

We will discuss alternative color schemes with our editor that are more easily seen by those with color deficiencies.

Figure Comment 5: “Figure 8: As Figure 7 – please consider using a different colour scale.”

We will discuss with the editor our options for different color scales to find the most appropriate for the publication.

Formatted: Normal, Line spacing: single

Page 27: [1] Formatted **Unknown**

Font: (Default) +Body (Times New Roman)

Page 27: [1] Formatted **Unknown**

Font: (Default) +Body (Times New Roman)

Page 27: [2] Deleted **LT Sean D. Egan, USN** **4/2/20 12:46:00 PM**

Page 27: [2] Deleted **LT Sean D. Egan, USN** **4/2/20 12:46:00 PM**